Local Data Integration over East-Central Florida Using the ARPS Data Analysis System

JONATHAN L. CASE AND JOHN MANOBIANCO

ENSCO, Inc., Cocoa Beach, and Applied Meteorology Unit, NASA, Kennedy Space Center, Florida

TIMOTHY D. ORAM AND TIM GARNER

Spaceflight Meteorology Group, NASA, Johnson Space Center, Texas

PETER F. BLOTTMAN AND SCOTT M. SPRATT

NOAA/National Weather Service, Melbourne, Florida

(Manuscript received 30 October 2000, in final form 31 August 2001)

ABSTRACT

The Applied Meteorology Unit has configured the Advanced Regional Prediction System (ARPS) Data Analysis System (ADAS) to support operational short-range weather forecasting over east-central Florida, including the Kennedy Space Center and Cape Canaveral Air Force Station. The ADAS was modified to assimilate nationally and locally available in situ and remotely sensed observational data into a series of high-resolution gridded analyses every 15 min. The goal for running ADAS over east-central Florida is to generate real-time analysis products that may enhance weather nowcasts and short-range (<6 h) forecasts issued by the 45th Weather Squadron (45 WS), the Spaceflight Meteorology Group (SMG), and the National Weather Service (NWS) at Melbourne, Florida (MLB). The locally configured ADAS has the potential to provide added value because it ingests all operationally available data into a single grid analysis at high spatial and temporal resolutions. ADAS-generated grid analyses can provide forecasters with a tool to develop a more comprehensive understanding of evolving fine-scale weather features than could be obtained by individually examining the disparate data sources.

The potential utility of this ADAS configuration to operational forecasters is demonstrated through a postanalysis case study of a thunderstorm outflow boundary that postponed an Atlas space launch mission, and a Florida cool-season squall line event. In the Atlas case study, a thunderstorm outflow boundary generated strong winds that exceeded the Atlas vehicle limits. A diagnosis of this event, using analysis products during the decaying phase of a Florida summer thunderstorm, illustrates the potential benefits that may be provided to forecasters supporting space launch and landing operations, and to NWS MLB meteorologists generating short-range forecast products. The evolution of analyzed cloud fields from the squall line event were used to track the areal coverage and tendencies of cloud ceiling and cloud-top heights that impact the evaluation of space operation weather constraints and NWS aviation products. These cases also illustrate how the analyses can provide guidance for nowcasts and short-range forecasts of Florida warm-season convection and fire-weather parameters. In addition, some of the sensitivities of the ADAS analyses to selected observational data sources are discussed.

Recently, a real-time version of ADAS was implemented at both SMG and the NWS MLB forecast offices. Future plans of this ADAS configuration include incorporating additional observational datasets and designing visualization products for specific forecast tasks. Finally, the ultimate goal is to use these ADAS analyses to initialize a high-resolution numerical weather prediction model run locally at SMG and the NWS MLB, in order to develop a cycling scheme that preserves fine-scale features such as convective outflow boundaries in short-range numerical forecasts.

1. Introduction

The recent development and implementation of many new in situ and remotely sensed observations has resulted in a wealth of meteorological data for weather forecasters. However, the forecaster's ability to manually integrate these data into a comprehensive analysis of the current state of the atmosphere is hindered by the volume of data and the differing characteristics of the various observing systems. Tools are needed to integrate and assimilate data routinely into a single system in order to simplify the analysis and interpretation of the state of the atmosphere while retaining the specific qualities of each data source. Therefore, in the near future,

Corresponding author address: Jonathan L. Case, ENSCO, Inc., 1980 N. Atlantic Ave., Suite 230, Cocoa Beach, FL 32931.
E-mail: case.jonathan@ensco.com.

weather forecasters should anticipate a transition towards analyzing ''processed observations'' in addition to the raw meteorological datasets (McPherson 1999).

One such data integration tool has been tailored for east-central Florida to support the National Aeronautical and Space Administration's (NASA) operations at the Kennedy Space Center (KSC) and the Cape Canaveral Air Force Station (CCAFS), and the National Weather Service (NWS) at Melbourne, Florida (MLB) forecast tasks. The Applied Meteorology Unit (AMU) at CCAFS configured the Advanced Regional Prediction System (ARPS) Data Analysis System (ADAS; Brewster 1996) to help meet the requirements for operational weather forecasting in east-central Florida. The mission of the AMU is to transition new and existing meteorological techniques and tools into operations for the U.S. Air Force 45th Weather Squadron (45 WS), the NWS Spaceflight Meteorology Group (SMG), and the NWS MLB (Ernst and Merceret 1995). The 45 WS provides weather support for ground and space launch operations primarily at KSC and CCAFS, aviation at Patrick Air Force Base, and space shuttle ferry flights (Boyd et al. 1995; Priselac et al. 1997). The NWS SMG provides weather support and forecasts for worldwide space shuttle landing sites including KSC and Edwards Air Force Base, California, and prepares local weather forecasts and services for the Johnson Space Center in Houston, Texas (Brody et al. 1997). As with other NWS offices across the nation, the NWS MLB is responsible for local public, aviation, fire-weather, and marine forecasts as well as warnings for hazardous weather in east-central Florida (Friday 1994). This paper will illustrate the potential utility that a locally configured analysis system such as ADAS can provide for the 45 WS, SMG, and NWS MLB operational forecasting needs, when combined with an appropriate visualization tool.

a. Background

Local analysis systems have been used for specific applications to improve nowcasts and short-range forecasts. The Local Analysis and Prediction System (LAPS; McGinley 1995) was run over the southeastern United States to provide special operational weather support for the 1996 Centennial Olympic Games in Atlanta, Georgia (Snook et al. 1998). LAPS generated surface analyses every 15 min and upper-level analyses every 30 min on a grid with 8-km horizontal and 50-mb vertical resolution. The LAPS analyses were used to initialize the Regional Atmospheric Modeling System (RAMS; Pielke et al. 1992; Walko et al. 1995), which provided numerical weather predictions on both an 8-km and a 2-km grid.

The LAPS is also the analysis package used operationally in the Advanced Weather Interactive Processing System (AWIPS) installed at all NWS forecast offices, including MLB and SMG. LAPS analyses are generated once per hour and are available 20–30 min past the valid time. The LAPS domain is approximately 600 km $\times$ 600 km, centered on the local forecast area with a horizontal resolution of 10 km. The most recent version (5.0) of AWIPS LAPS has an adjustable domain. LAPS uses the Rapid Update Cycle (RUC) model for its background field with an ability to use the Eta Model in instances where the RUC is unavailable. Datasets currently incorporated into the LAPS at NWS MLB and SMG include Aviation Routine Weather Report (METAR) and buoy data, *Geostationary Operational Environmental Satellite-8* (*GOES-8*) infrared imagery, and the lowest tilt of Level III reflectivity data from the MLB Weather Surveillance Radar-1988 Doppler (WSR-88D). Future versions of LAPS on AWIPS may incorporate visible satellite imagery and the full-volume scan radar data including radial velocity information.

The Integrated Terminal Weather System (ITWS) is another local analysis system that focuses on the environment within the airport terminal area. ITWS was designed to provide weather products for air traffic automation systems at high resolutions in both space and time (Evans and Ducot 1994). The ITWS integrates Terminal Doppler Weather Radar data, available Federal Aviation Administration and NWS sensors, aircraft observations, and numerical model output. A prototype ITWS gridded wind product was tested in central Florida for the Orlando International Airport and run on a 2-km fine-scale grid with a 5-min update cycle (Cole and Wilson 1995).

The Center for Analysis and Prediction of Storms (CAPS) ran a local analysis and forecasting system in support of aviation weather forecasts for American Airlines (AA). As part of a research partnership with AA, CAPS generated real-time analyses and forecasts at the University of Oklahoma using the ARPS Numerical Weather Prediction (NWP) model (Xue et al. 2000, 2001). With an emphasis on the major AA hubs of Dallas–Fort Worth (DFW) and Chicago–O'Hare, project ''Hub-CAPS'' created real-time analysis and forecast products over the southern plains and DFW area with resolutions of 27 km and 9 km, respectively. ADAS produced gridded analyses every hour whereas the ARPS model ran four times per day on the 27-km grid and once per day on the 9-km grid (Carpenter et al. 1999).

Each of the studies described above generated analyses by using a background or first-guess field from a large-scale NWP model such as the RUC (Benjamin et al. 1998) or Eta (Rogers et al. 1996). In LAPS–RAMS and project Hub-CAPS, the analyses were subsequently used as a ''cold-start'' initialization for the local-scale forecast models. As an alternative method, analyses and forecasts may be cycled by using short-range local NWP forecasts as background fields for ensuing analyses. By cycling a high-resolution NWP model with an analysis system such as ADAS, mesoscale details resolved by the local model can be retained in subsequent analyses. In addition, kinematic and thermodynamic fields in the

model initial condition will be in closer balance than with a ''cold start'' analysis field.

b. Local data integration in east-central Florida

In this study, the AMU evaluated the utility of local data integration by configuring only the data assimilation portion of the ARPS NWP model. Results from these high-resolution analyses are presented along with a discussion of the potential operational utility of a real-time ADAS over east-central Florida. NWP forecasts or cycling as described above are beyond the scope of the original study and are not addressed. Nevertheless, the results presented in this paper may serve as an impetus for future work involving local-scale NWP modeling and cycling over east-central Florida.

The motivation for running ADAS in east-central Florida emerged from two primary factors. First, KSC/CCAFS and the immediate surrounding areas have a dense network of disparate meteorological observations including a mesonetwork of 47 wind towers and 6 Doppler radar wind profilers. This mesonetwork provides the forecaster with detailed information at frequent time intervals; however, forecasters are challenged with integrating this information to develop a conceptual understanding of the current state of the atmosphere. Second, space launch and landing operations at KSC/CCAFS and short-term forecasting concerns at the NWS MLB require detailed forecasts of cloud ceilings, cloud-top temperatures and heights, winds, and hazardous weather such as thunderstorms. By automatically integrating the disparate data into a single analysis at frequent time intervals, ADAS can simplify the process of developing a comprehensive understanding of the current state of the atmosphere and monitoring the temporal evolution of the atmospheric conditions. Proper visualization of the resulting grid analyses can produce derived products tailored to analyzing and forecasting local weather conditions, including those critical for space operations.

The ultimate goal for running ADAS over east-central Florida is to generate products in real time that may enhance a forecaster's understanding of the state of the atmosphere in order to improve weather nowcasts and short-range forecasts. The locally configured ADAS can provide added value because it incorporates operationally available data in east-central Florida and it is run at finer spatial and temporal resolutions than current national-scale operational model analyses. This design of ADAS is similar to the function of LAPS in AWIPS; however, this ADAS configuration also integrates additional datasets not currently available in AWIPS. Running ADAS over east-central Florida simplifies the short-range forecasting process by providing a consistent platform for viewing real-time data.

The configuration and implementation of ADAS for east-central Florida was conducted in a three-phased effort. First, the AMU documented all existing meteorological data sources around central Florida that could be incorporated into ADAS, configured the ADAS software to generate high-resolution gridded analyses in space and time, and demonstrated the fidelity and potential operational utility of the prototype ADAS by examining a Florida warm- and cool-season case study (Manobianco and Case 1998). Next, the AMU simulated a real-time configuration of ADAS for a period of two consecutive weeks using data saved at SMG and the NWS MLB during February 1999 (Case 1999). Finally, a real-time version of the prototype ADAS was installed at both the SMG and NWS MLB offices.

The objective of this paper is to highlight the potential utility of using ADAS in support of space launch and landing operations at KSC/CCAFS, as well as demonstrate the added value of utilizing these locally configured analyses for NWS short-range forecast products. A warm-season case study from 26 July 1997 is presented to illustrate the value of utilizing ADAS analyses in monitoring strong convective outflow winds. Another case from 28 February 1999 is presented as an example of how the analysis products can be used to diagnose various cloud properties associated with the advancement of a squall line across central Florida. The subsequent sections of this paper are organized as follows. Section 2 presents some of the challenges of short-range weather forecasting in east-central Florida that could be simplified by utilizing ADAS analyses. Section 3 discusses the methodology, the prototype ADAS, and the selection of case and sensitivity studies. Section 4 describes the characteristics of the datasets that were archived and used to simulate a real-time ADAS configuration. Section 5 illustrates the potential utility of the prototype ADAS to forecasters by presenting analysis results from the 26 July 1997 case study and a prefrontal squall line that occurred on 28 February 1999. Section 6 shows results from data sensitivity tests. Finally, section 7 summarizes the paper.

2. Short-range forecast challenges in east-central Florida

a. Weather constraints on space operations at KSC/CCAFS

Space launch, space shuttle landings, and ground-support operations at KSC/CCAFS are subject to a wide variety of weather restrictions to ensure personnel safety, vehicle safety, and launch success. Because of the high frequency of thunderstorms in central Florida, particularly from May to September, lightning is one of the primary weather concerns at KSC/CCAFS. Lightning Launch Commit Criteria (LCC) consist of eleven specific rules that have been developed to protect both manned and unmanned vehicles against natural and triggered lightning threats (Roeder et al. 1999). The LCC place restrictions on a wide range of weather conditions that can lead to natural or triggered lightning including

TABLE 1. A subset of the weather constraints that restrict space shuttle landings (NASA–JSC 2000).

Weather constraint	Threshold	Purpose
Ceiling	>8000 ft	Provide astronaut commander sufficient time to visually acquire runway and landing aids.
Thunderstorms (including attached nontransparent anvils and cumulus clouds above −20°C) and precipitation	None with 30 n mi of center of runway or within 10 n mi horizontally of flight path	1) Avoid damage to vehicle by natural or triggered lightning. 2) Avoid structural damage and control problems due to turbulence. 3) Avoid damage to thermal control system (heat tiles).
Detached nontransparent anvils less than 3 h old	None within 20 n mi of center of runway or within 10 n mi horizontally of flight path	Avoid damage to vehicle by natural or triggered lightning.

the recent occurrence of lightning, cumulus clouds with cloud tops reaching the water mixed-phase region (~0° to −20°C), attached and detached anvil clouds, debris clouds, clouds with thickness greater than 1372 m (4500 ft) within the mixed-phase region, smoke plumes, and hazardous atmospheric electric fields. If any LCC is violated during the launch window, then the launch is delayed until weather conditions permit the launch, or postponed to another day. Operational forecasters use these LCC during every launch countdown to assess the potential for natural and triggered lightning. In addition to the LCC restrictions during all launch operations, forecasters also closely monitor the surface wind speed and wind direction because each vehicle is subject to specific wind constraints based on the stresses that the vehicle can sustain.

The space shuttle manned vehicle has a variety of flight rules (FR) designed to ensure the safety of flight and landings, taking into account the maneuverability of the shuttle, slant range visibility considerations, protection against tile damage, and protection against natural and triggered lightning (Brody et al. 1997; NASA–JSC 2000). SMG forecasters are responsible for issuing all landing forecasts for the space shuttle missions. Table 1 contains a subset of some particular rules related to clouds, thunderstorms, and precipitation. Two of the most important forecasts are the prelaunch return-to-launch-site forecast and the deorbit burn landing forecast issued about 35 min and 90 min, respectively, prior to the expected landing time. Forecasters must use data throughout much of the Florida peninsula and offshore waters to evaluate the FR to develop an accurate forecast. This large evaluation region is necessary given the 90-min time from the issuance of the deorbit burn forecast to the time of landing, and the area over which some weather conditions must be acceptable [30 n mi (55.6 km) radius around KSC]. Given the complexity and time constraints associated with evaluating LCC and FR and generating short-range forecasts, both SMG and 45 WS forecasters could benefit from the simplifications provided by real-time ADAS analysis products that integrate all available observational data in east-central Florida.

b. National Weather Service short-range forecasts

The NWS MLB office has a wide range of short-range analysis and forecasting responsibilities that require the issuance of time-constrained advisories and warnings, amendments, and forecasts. One of the biggest forecast challenges in east-central Florida, particularly during the summer months, is predicting the location, timing, and subsequent intensity of convection. The accurate placement of low-level mesoscale boundaries is crucial during the Florida summer months when sea, river, and lake breezes interact with existing thunderstorm outflow boundaries, resulting in convective initiation (Wilson and Megenhardt 1997). Standard aviation products, short-range forecasts, and county-specific warnings require extensive analysis of the current conditions to monitor the evolution of such mesoscale boundaries.

The NWS MLB also issues Terminal Aerodrome Forecasts (TAF) for aviation operations and fire-weather spot forecasts to assess wildfire hazards and weather risks. Both of these products typically involve nowcasts and short-range forecasts of specific parameters requiring knowledge of the existing state of the atmosphere. The TAF criteria (a subset shown in Table 2 for cloud ceilings) include a wide range of rules according to the development and evolution of parameters such as cloud ceilings, visibility, present weather, wind direction, wind speed, and low-level wind shear (NWS 1997). Fire-weather spot forecasts are produced when requested by fire agencies during wildfires, or by federal agencies prior to or during prescribed burns (NWS 2000). Each spot forecast contains expected surface weather conditions at an hourly or bihourly frequency, and includes temperature, relative humidity, wind direction, wind speed, and probability of precipitation. Forecasts of transport wind direction and speed, mixing height, and dispersion index are also provided to fire agencies. Specific details concerning wind shifts, sudden speed changes, and cloud-to-ground lightning are especially important. Two case studies are presented in section 5 that will provide examples of how ADAS analyses can be used by forecasters to simplify the assessment of

TABLE 2. The criteria used by the NWS for generating cloud ceiling TAF (NWS 1997).

If ceiling forecast is:	Amend if ceiling:
No ceiling or ceiling above 3000 ft.	In the forecaster's judgment the forecast is not representative, or the ceiling falls to 3000 ft or below.
3000 to 2000 ft.	Increases to greater than 3000 ft, or falls below 2000 ft.
Less than 2000 to 1000 ft.	Increases to equal or exceed 2000 ft, or falls below 1000 ft.
Less than 1000 to 600 ft.	Increases to equal or exceed 1000 ft, or falls below 600 ft.
Less than 600 to 200 ft.	Increases to equal or exceed 600 ft, or falls below 200 ft.
Less than 200 ft.	Increases to 200 ft or more.

some of the specific forecast criteria described above during space launch and NWS MLB operations.

3. Analysis configuration

a. ADAS software

ADAS was designed by CAPS personnel to assimilate a wide range of observed data to provide specialized analyses for initializing the ARPS NWP model (Brewster 1996). ADAS has been used to generate mesobeta scale analyses (~10–30 km) by assimilating a multitude of data including aircraft, radar, profiler, satellite, surface, and rawinsonde observations (Droegemeier et al. 1996). With most ADAS data input capabilities already in place, the AMU modified and wrote some additional data-ingestion programs to incorporate specialized local data such as wind towers and Doppler radar wind profilers, and to conform with local data formats at KSC/CCAFS. Details on some of the features of ADAS are provided below.

In order to compute gridded fields of temperature, moisture, and other variables, ADAS utilizes the Bratseth objective analysis procedure (Bratseth 1986) consisting of a modified iterative successive corrections method (SCM) that converges to the statistical or optimum interpolation (OI; Gandin 1963). In the SCM, an analysis is created from a background or first-guess grid and a set of observational data. A background grid typically consists of a large-scale model initialization, analysis, or short-term forecast. The variables at specific grid points are modified from the background values by computing and summing observational increments for data within a specified distance of the grid points. An observational increment is weighted according to its distance from the grid point, the local data density, the expected observation error relative to the background and other observations, and specified mathematical relationships that estimate the correlation of increments as a function of horizontal and vertical distance. The sum of these weighted observational increments is applied to the background field to generate a new analysis value at the grid point. This process is repeated for all grid points in order to generate the new analysis grid.

The procedure described in the preceding paragraph represents one iteration or pass of the SCM. Several passes can be applied to the background grid in order to fit the observational data more closely or to incorporate different data sources for each pass. During each successive pass, the old analysis value at each grid point becomes the new background value as the observational-increment procedure is repeated.

Bratseth is superior to a traditional SCM because the Bratseth algorithm accounts for variations in data density and observational errors, similar to OI. When there is an expectation of a balance between wind and mass (e.g., geostrophy), a multivariate OI scheme can also account for the correlation between the wind and mass increments, but can be computationally more expensive than the SCM. The Bratseth scheme realizes some advantages of OI while retaining the computational efficiency of a SCM.

In the version of ADAS used in this study, the software analyzes five variables at each model vertical level: u- and v-wind components, pressure (p), potential temperature (θ), and RH*. Here, RH* is a moisture variable analogous to dewpoint depression and is defined as

$$\text{RH}^* = \sqrt{1.0 - \text{RH}}, \tag{1}$$

where RH is the relative humidity (Brewster 1996). The ARPS/ADAS vertical coordinate is a terrain-following height coordinate analogous to the traditional sigma coordinate.

One of the features available from ADAS is the Complex Cloud Scheme (CCS) which serves as the basis for moisture data assimilation in the ARPS model (Zhang et al. 1998). The CCS is based on the cloud analysis algorithms of LAPS (Albers et al. 1996) and includes some modifications. The CCS incorporates a variety of data and derives a number of cloud and moisture products using empirical rules based on satellite, radar, and surface data. A portion of the scheme uses a Barnes (1964) analysis to spread point-wise observations.

The data used by the CCS include METAR cloud observations, satellite infrared and visible imagery, and radar reflectivity. The products derived from these data include three-dimensional (3D) cloud cover, fractional cloud cover, cloud liquid water (q_c) and cloud ice water (q_i) mixing ratios, cloud and precipitation types, in-cloud vertical velocity, icing severity index, rain/snow/hail mixing ratios (q_r, q_s, q_h), cloud base, cloud top, and cloud ceiling fields. Furthermore, the CCS enhances the specific humidity (q_v) within areas of analyzed clouds. Some of the empirical products available from the CCS such as cloud ceilings and cloud-top heights

are examined in this paper to determine the potential benefit to operational forecasting at SMG and the NWS MLB. More details of the CCS can be found in Zhang et al. (1998).

b. ADAS quality control

ADAS contains two algorithms to handle the quality control (QC) of data incorporated by the analysis scheme. One QC method involves a two-step procedure to check surface observations. First, a time-continuity test is applied to each surface observation to ensure that it is not drastically different from the previous hourly value. The hourly differences are computed for all stations and for all variables. If any data value lies outside of four standard deviations from the mean of the average hourly differences, then the observation is rejected. This temporal check could result in occasional rejection of good surface data, particularly during isolated convective events when only a small fraction of surface observations may be affected by an outflow boundary or precipitation-cooled air.

Second, the surface data undergo a spatial continuity check. A Barnes objective analysis is performed at the station location using surrounding surface observations. A weighted mean and standard deviation are computed based on these surrounding observations. If the data value in question lies outside of three standard deviations from the analyzed value at the observation location, then the observation is rejected.

For upper level data QC, ADAS compares all observations to the background grid values interpolated to the observational location. A difference is computed between the observation and the interpolated background value and this difference is compared to predetermined thresholds for each data source except for surface data. Data that result in differences outside of these threshold bounds are rejected prior to the analysis computation.

c. Analysis grid configuration

A nested-grid configuration was used for generating high-resolution analyses similar to the ITWS (Cole and Wilson 1995). ADAS was run every 15 min at 0, 15, 30, and 45 min past the hour over outer and inner grids with horizontal resolutions of 10 km and 2 km, respectively. For the simulated real-time configuration, 3–6-h forecasts from the RUC model were used as background fields for the 10-km ADAS analyses. The RUC forecasts, interpolated to an 80-km grid with vertical levels every 50 mb from 1000–100 mb, were utilized for this study. RUC forecasts were linearly interpolated in time every 15 min for each 10-km analysis cycle. In the event of missing RUC forecasts, no analyses were generated for this experiment; however, in the real-time ADAS configuration currently running at SMG and the NWS MLB, older RUC forecast grids (6–12-h forecasts) serve as background fields for the 10-km analysis. The resulting 10-km analyses were subsequently used as background fields for the 2-km analyses.

The 10-km (2-km) analysis grid covers an area of 500 km $\times$ 500 km (200 km $\times$ 200 km) and contains 30 vertical levels that extend from near the surface to about 16.5 km above ground level. The terrain-following vertical coordinate is stretched such that the finest resolution (20 m) occurs near the ground, whereas the coarsest resolution ($\sim$1.8 km) occurs at the top of the domain. The horizontal coverage and gridpoint distributions for both the 10-km and 2-km analysis grids are shown in Fig. 1. The grid configuration was chosen based on the operational requirements for domain coverage, cycle run time, and computational resources available when the configuration was first established. Counties over east-central Florida are denoted in Fig. 1b as a reference for discussions in section 5.

d. Visualization of analysis products

An important component of this analysis configuration is to provide forecasters with the capability to generate and display routine graphical products in real time. As a result, the analysis cycle includes a step to convert the ADAS analyses to the data format of the General Meteorological Package (GEMPAK) analysis and display software (desJardins et al. 1991), using a conversion utility available within the ARPS distribution package. Once the 10-km and 2-km ADAS analyses are completed, the data are interpolated to constant pressure and height surfaces and written to GEMPAK grid files. A wide variety of plan views, cross sections, time animations, and time–height cross sections of the analyzed meteorological parameters can be examined using the GEMPAK Analysis and Rendering Program (GARP) graphical user interface (GUI). Both SMG and the NWS MLB offices currently use the GARP GUI to display and manipulate real-time analysis products.

4. Data characteristics

a. Coverage and resolution

Numerous observational data sources with differing characteristics are available in east-central Florida. Data density and coverage vary considerably depending on the level in the atmosphere and distance from KSC/CCAFS. All observational data within 250 km of KSC/CCAFS that can be incorporated by ADAS are listed in Table 3. This table includes an estimate of the horizontal resolution, vertical extent, frequency of observation, real-time latency, and the variables that are measured for each data source. The KSC/CCAFS mesonetwork of wind tower and profiler observations, WSR-88D data, and *GOES-8* infrared and visible satellite imagery provide the highest-resolution observations in both space and time across east-central Florida. It is

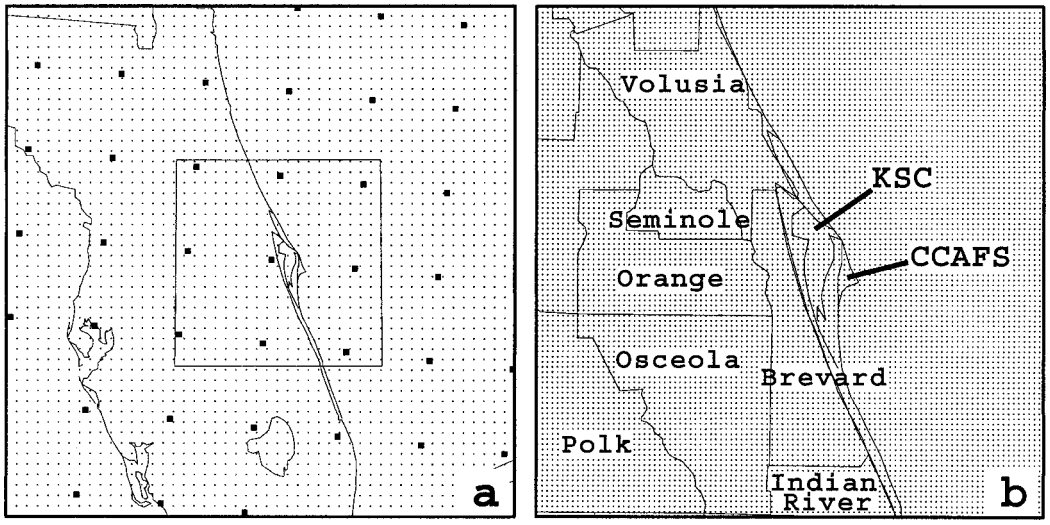

FIG. 1. The ADAS domains for (a) the 10-km grid and (b) 2-km grid. (a) The 10-km grid point (small dots) and 80-km RUC grid-point locations (solid squares), and (b) the 2-km grid-point locations (small dots) and county labels are shown. The boxed region in (a) denotes the 2-km domain.

important to note that among the measured variables in east-central Florida, moisture is the least represented.

The horizontal distribution of WSR-88D and KSC/CCAFS observations over the Florida peninsula and east-central Florida are shown in Fig. 2. For the 26 July 1997 case, Level II WSR-88D data from only the MLB site were ingested. For the simulated real-time ADAS configuration during 15–28 February 1999, Level III WSR-88D products (Klazura and Imy 1993) from all Florida radar sites were used in creating the analyses. SMG does not currently receive the MLB Level II WSR-88D data in real time; instead, SMG obtains Level III WSR-88D products in real time from a next generation radar (NEXRAD) Information Dissemination Service (NIDS) vendor.

Several types of radar products are available in the Level III format; however, these products have limitations compared to the full-resolution Level II WSR-88D data. Currently, ADAS has the capability to ingest only reflectivity and radial velocity products from the suite of available Level III WSR-88D products. Only the lowest 4 elevation angles of reflectivity and radial velocity data are available in Level III WSR-88D data, as opposed to 14 elevation angles with Level II data using volume coverage pattern 11. The horizontal resolution of the Level III data at SMG is slightly degraded, since they receive data on a 1 km $\times$ 1 km pixel format from a NIDS vendor, whereas Level II radial velocity data have 225-m gate-to-gate resolution. The temporal frequency of Level III data is the same as Level II data. The products that were archived by SMG for the simulated real-time ADAS configuration include reflectivity and radial velocity data for the four lowest elevation angles at the MLB WSR-88D, and the two lowest elevation angles at all other Florida radar sites [Tallahassee (TLH), Jacksonville (JAX), Tampa Bay (TBW), Miami (AMX), and Key West (BYX)].

The coverage of the MLB WSR-88D includes all of the 2-km domain and a large portion of the 10-km domain (Fig. 2a). However, data from several other Florida radar sites also cover portions of the 10-km domain (TLH, JAX, TBW, and AMX) and even the 2-km domain (TBW and JAX). Because each of the WSR-88D Level III products used in this study has a range of 230 km, the additive effect of all radar sites in the Level III dataset results in nearly continuous horizontal coverage of reflectivity and radial velocity data at low-levels on the 10-km and 2-km analysis grids. Despite this improvement in horizontal coverage using Level III data, it will be shown in section 6 that the decrease in both horizontal resolution and vertical coverage of Level III data leads to a degradation in the quality of the analyses.

b. Data latency

When configuring ADAS for an operational implementation, an important issue to consider is the lag that occurs between the time of observation and the time that the data are received at a local office. The type and amount of data that should be ingested largely depend on the scales of motion to be sampled and the cycle time of the integration system. Because ADAS was tailored to provide mesoscale analyses at 15-min intervals, the most valuable real-time data sources provide observations at least as often as the analysis cycle; however, if data that experience significant time lags are ingested into ADAS, then outdated information would be incorporated. Ingesting outdated data could degrade the quality of the analyses, especially associated with

TABLE 3. Data availability within 250 km of KSC/CCAFS including data type, horizontal resolution, vertical extent, variable(s) observed, observation frequency, and real-time lag. The real-time lag represents the time between observation and receipt of data at SMG.

Data type	Horizontal resolution	Vertical extent	Variables	Frequency (min)	Real-time lag (min)
RUC forecast	80 km	1000–100 mb	u, v, T, RH, heights	180	150–180
GOES-8 VIS imagery	1 km	—	Brightness T	15	5
GOES-8 IR imagery	4 km	—	Brightness T	15	5
Cloud/water vapor drift winds	24 km	Variable	u, v	360	120
Sfc reports	34 km[a]	Sfc	u, v, T, T_d, p	60	10
KSC/CCAFS towers	4 km	1.8–150 m	u, v, T, RH	1	1–2
Florida rawinsondes	200 km	Sfc to stratosphere	u, v, T, RH, p	720	≥120
CCAFS rawinsonde	N/A	Sfc to stratosphere	u, v, T, RH, p	Variable	20
GOES-8 soundings	30 km	Sfc to stratosphere	T, q	60	50
Level II WSR-88D	0.2–1.0 km	Variable[c]	Radial wind, reflectivity, spectral width	5–10	<1[d]
Level III WSR-88D	1.0 km	Variable[c]	Radial wind, reflectivity, spectral width	5–10	3–5
Aircraft/pilot reports	Variable	Variable	u, v, T, icing, turbulence, cloud	Variable	5–30
ACARS[e]	25 km	Variable	u, v, T	7.5	15[f]
915 MHz profiler	11 km[b]	0.117–3.1 km	u, v, T_v	15	1–2
50 MHz profiler	11 km[b]	2.0–18.6 km	u, v	5	1–2

[a] Represents the combined horizontal resolution of METAR, buoy/ship, and the central Florida mesonet.
[b] The combined horizontal resolution of five KSC/CCAFS 915-MHz profilers and one 50-MHz profiler.
[c] Depends on radar volume coverage pattern.
[d] Melbourne, FL, NWS office only (D. Sharp 1999, personal communication).
[e] ACARS = Aeronatuical Radio, Inc. (ARINC) Communications, Addressing and Reporting System.
[f] Estimated for ACARS data obtained from the Forecast Systems Laboratory.

rapidly evolving mesoscale features such as deep convection and outflow boundaries.

The right-hand column of Table 3 provides a summary of the estimated time lags for each real-time data source as received locally at SMG and the NWS MLB. The AMU identified cloud and water vapor drift–derived winds, *GOES-8* soundings, and Florida rawinsondes [with the exception of Cape Canaveral (XMR)] as having substantial time lags. Based on several considerations, these data were excluded from the simulated real-time configuration of ADAS. First, cloud and water vapor drift–derived winds (120 min), *GOES-8* soundings (50 min), and Florida rawinsondes (120 min) experience time lags significantly larger than the analysis cycle time (15 min). Second, the ADAS software does not currently have the capability to time-weight observational data. Finally, Florida rawinsondes and *GOES-8* derived winds are currently ingested into the RUC hourly data assimilation cycle (Benjamin and Brundage 2001). Therefore, these two data sources already have an indirect impact on the analyses through the RUC background fields.

c. Data ingest

Observational data were ingested into ADAS at times closest to the valid analysis time within a 15-min window centered on the analysis time (±7.5 min). In a real-time configuration, data ingest for each cycle would begin after the valid analysis time to allow for the transmission, receipt, and processing of real-time data. This particular strategy was utilized in the simulated real-time configuration because each analysis cycle consists of observations grouped as closely together in time—making the analysis as representative as possible. An alternative data ingest configuration is to start each cycle at the actual analysis time and incorporate all data collected since the previous cycle. However, this data ingest configuration could result in a less representative mesoscale analysis because observational data would be spaced farther apart in time.

Since the analysis cycle was run every 15 min over very fine scales, it was necessary to ingest some data using nonstandard methods. The local XMR rawinsonde data were ingested in a unique manner in order to account for the specific location of the balloon during ascent. For synoptic-scale analyses, rawinsondes are assumed to provide vertical profiles of moisture, temperature, and winds at a single time and location. However, the balloon can drift a significant distance from the launch site during ascent depending on the speed and direction of the environmental wind. Furthermore, balloons used for upper-air measurements ascend at a rate of about 5 m s^{-1} so observations are collected over a period of about 1 h. To account for balloon drift, the XMR rawinsonde data were treated as single-level observations each with an appropriate horizontal and vertical location determined by using the ascent rate and observed winds. These single-level rawinsonde observations were then grouped into 15-min bins centered on

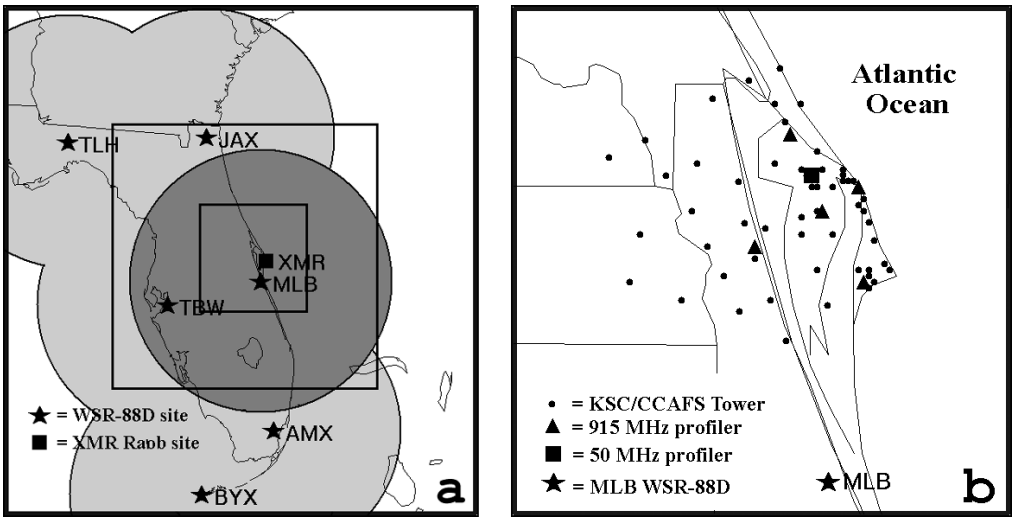

FIG. 2. The distribution of WSR-88D data and KSC/CCAFS observations in the simulated real-time configuration are shown over the Florida peninsula and east-central Florida, respectively. (a) The dark shading represents the areal coverage of the MLB WSR-88D whereas the light and dark shading collectively represent the areal coverage of all Florida radar sites. Outlines of the (outer) 10-km and (inner) 2-km analysis domains and the location of the XMR rawinsonde are also shown. (b) The locations of the KSC/CCAFS towers, 915-MHz and 50-MHz profilers, and the MLB WSR-88D are shown.

each analysis time. As a result, only a segment of the rawinsonde profile was used for each analysis cycle.

d. ADAS radar remapper

Radar observations from the WSR-88D are remapped onto the ADAS analysis grid by averaging all reflectivity and radial velocity data that fall in each grid volume as described by Brewster (1996) and Albers (1995). The size of an individual grid volume is determined by the local grid spacing centered on the point in question. Currently, spectrum width data from the WSR-88D are not used by ADAS. Radar observations in a grid volume are rejected if the data cover an insufficient percentage of the grid volume or the radar observations have a high variance within the grid volume. The radar data that have sufficient coverage and small variances are remapped to the analysis grid and stored as vertical columns identified by latitude and longitude. This remapping algorithm serves as a means to thin out dense data to the resolution of the analysis grid. A similar remapping procedure was used for *GOES-8* visible and infrared satellite data on the 10-km and 2-km grids. The remapped satellite data subsequently enhanced the analysis of clouds by the CCS procedures as discussed in section 3a.

The reflectivity data remapped to the analysis grid are used to enhance the background cloud and moisture fields in two ways. First, reflectivity values greater than 20 dBZ are used to enhance the 3D relative humidity field of the background field. Second, reflectivity values above 25 dBZ are used to increase cloud water in the analysis (Brewster 1996). These enhancements in the analysis grid provide an NWP model with an initial condition that reduces model spinup time for saturation and precipitation in areas of ascent.

Radial velocity data from the WSR-88D are converted to observational increments of the u- and v-wind components and assigned a direction along the radar's azimuth. When two radars affect the same analysis grid volume, the radial wind data are correlated according to the local difference in the azimuth angle between the two radar beams. The radial velocities within each grid volume are compared to each other and if the data overlap more than one Nyquist interval, the radial winds are unfolded accordingly. The unfolded winds are then compared to the background field and rejected if the radar winds differ from the background wind field by a user-specified threshold. The u- and v-wind observational increments from the radial velocities are analyzed to the grid on a separate pass after all in situ observations have been incorporated. This radar remapping algorithm is run individually for both the 10-km and 2-km analysis grids.

As a result of the radar characteristics, the analyzed wind field using WSR-88D radial velocity data are somewhat biased to an orientation parallel to the resultant wind flow. For example, if southwesterly flow was observed by the WSR-88D and these observations were significantly different than the background wind field, the resulting analysis would be most representative to the southwest and northeast of the radar site. However, it is important to note that the ADAS algorithm modifies the local transverse wind component in the analysis as well. To obtain wind information perpendicular to the radar beam orientation, ADAS combines radial velocity observations along adjacent radials when generating the wind analysis (Brewster 1996).

The remapped WSR-88D data were ingested into ADAS based on the time of the volume scan relative to the analysis time. In precipitation mode, the WSR-88D requires approximately 5 min to complete a full-volume scan. As a result, each analysis cycle was designed to incorporate the radar scan that begins before the analysis time and overlaps the analysis time.

5. Potential utility to forecasters

This section presents analysis results for two separate case studies using graphical products generated by GEMPAK utilities. These cases are shown to provide examples of how the prototype ADAS analyses could be utilized by SMG forecasters to monitor weather constraints associated with space shuttle landing forecasts, and by 45 WS forecasters to examine weather constraints during ground and space launch operations. Furthermore, these cases provide examples of how ADAS could assist NWS MLB meteorologists in generating short-range forecast products for east-central Florida such as TAF and fire-weather forecast products. First, the diagnosis of a convective outflow boundary that postponed an Atlas rocket launch on 26 July 1997 is presented. Cloud analysis products from the 28 February 1999 case study of a prefrontal squall line are shown thereafter. In both cases, the results are taken from the 2-km analysis grid.

a. 26–27 July 1997 case study: Diagnosis of an outflow boundary

A typical, undisturbed Florida warm-season environment characterized the 26–27 July 1997 case. A large area of surface high pressure was located over the Midwest extending eastward across the southeast United States (not shown). A weak pressure trough oriented north–south was located along the eastern seaboard. Low- to midtropospheric mean wind flow across central Florida was generally southwesterly at less than 5 m s^{-1}. Relatively moist and unstable conditions resulted in the development of scattered thunderstorms across the peninsula during the early afternoon hours. At the same time, a sea breeze boundary developed along the east coast of Florida. Later in the afternoon, strong thunderstorms developed southwest of KSC/CCAFS and generated an outflow boundary that propagated northeastward across KSC/CCAFS. This outflow boundary caused winds greater than 15 m s^{-1} as noted on the KSC/CCAFS mesonet towers around 2245 UTC 26 July.

An Atlas space launch mission from CCAFS was scheduled for 0054 UTC 27 July 1997. This particular launch had a surface wind restriction at liftoff of 12.4 m s^{-1} (24 kt) for winds from 16°–294°; however, if the wind direction was from 295°–15°, the restriction was 11.9 m s^{-1} (23 kt). By 2308 UTC, the launch attempt was postponed for the day due to high winds and new thunderstorm development associated with the outflow boundary. This case study was chosen due to the rapidly changing weather features and operational significance of the event.

The evolution of the ADAS-analyzed wind speeds and wind vectors at 480 m (Fig. 3) clearly illustrates the formation and intensification of the outflow boundary during the late afternoon of 26 July 1997. Wind speeds greater than 8 m s^{-1} develop over the Brevard–Osceola County border at 2215 UTC 26 July (Fig. 3a) and spread out radially over the next 45 min. By 2245 UTC, the maximum analyzed winds ($>$12 m s^{-1}, exceeding the Atlas vehicle threshold) move northeastward into KSC/CCAFS and offshore regions of central Brevard County (Fig. 3c). Examination of Level II radar reflectivity and radial velocity data (not shown) indicate that features present in the high-resolution wind analyses of Fig. 3 are consistent with the scale and motion of patterns associated with the observed thunderstorm. Forecasters have noted that these displays of the total wind from the grid analyses are easier to interpret quickly than radial velocity products from the WSR-88D.

Cross sections taken along lines oriented southwest–northeast in Fig. 3 help to illustrate the vertical structure and evolution of wind speeds analyzed on the 2-km domain. A core of relatively strong winds (8–10 m s^{-1}) associated with the convection to the southwest of KSC/CCAFS extends from near the surface to 3000 m at 2215 UTC (Fig. 4a). At 2230 UTC, a separate low-level wind maximum with speeds greater than 6 m s^{-1} develops between 200 and 500 m ahead of this core (Fig. 4b). Fifteen minutes later, this low-level wind maximum advances northeastward (left-to-right along the cross section) and increases in intensity to greater than 10 m s^{-1} (Fig. 4c). By 2300 UTC, the winds between 1000 m and 3000 m weaken but the low-level wind maximum maintains its intensity. Also at this time, a third wind maximum becomes evident in the 0–200-m layer on the right side of Fig. 4d.

Above 200 m, surface-based observations do not influence the analyses due to the vertical correlation range used in this particular ADAS configuration (refer to Table A1 in the appendix). Thus, changes in the horizontal wind field above 200 m are primarily caused by WSR-88D radial velocities in areas where radar targets are available. The wind maximum between 200–500 m at 2300 UTC (Fig. 4d) shows a gradual upward tilt from southwest to northeast (left to right). This feature results from the incorporation of radar data which slopes upward away from the radar site. Furthermore, note that the winds are less than 6 m s^{-1} between the tilted wind maximum and the wind maximum in the lowest 200 m. These weaker winds are located at levels below the influence of radar data but above the influence of near-surface KSC/CCAFS tower data. Therefore, the weaker background winds from the 10-km analysis are retained and the two features are distinct. However, by increasing

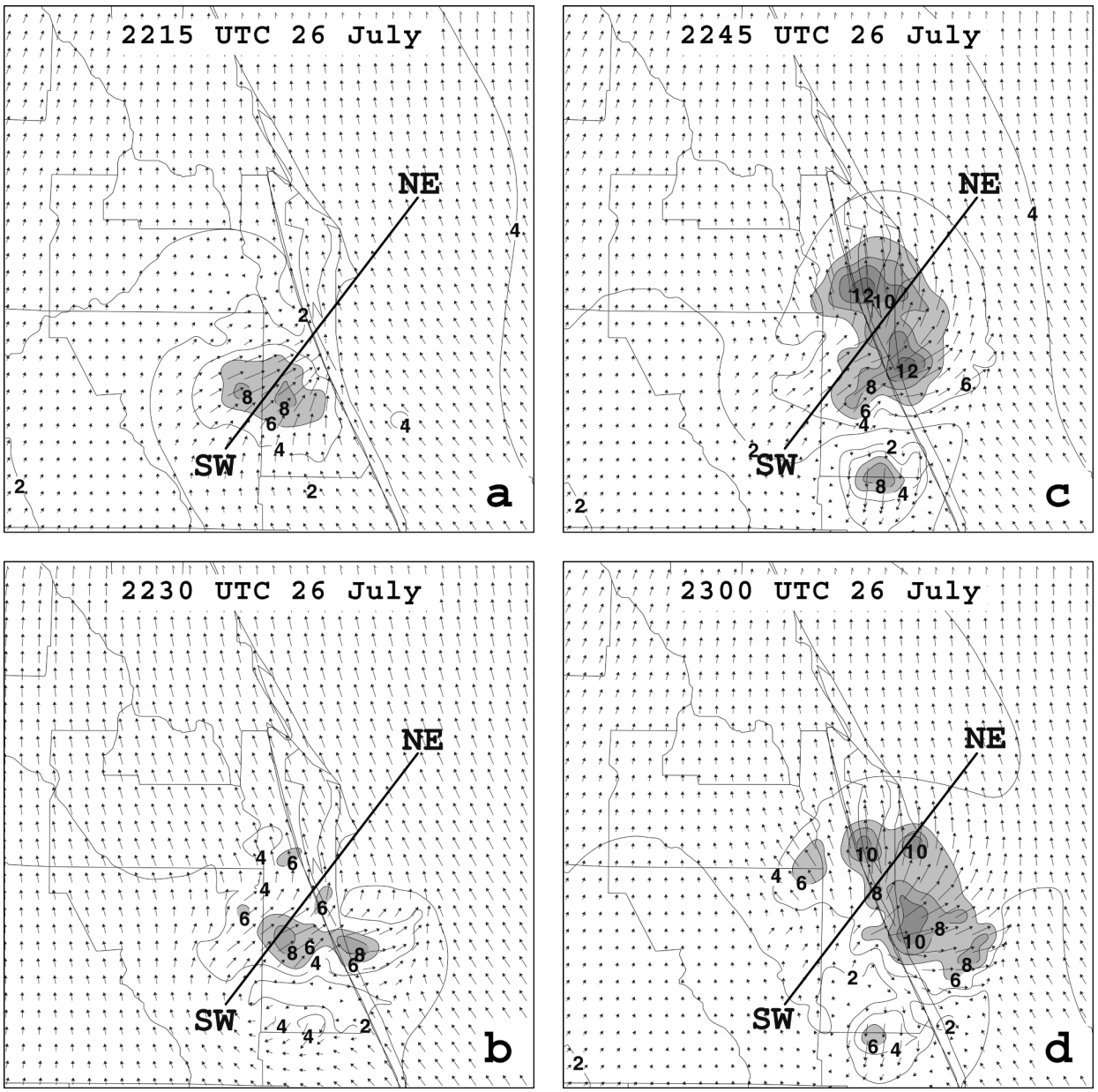

FIG. 3. A display of the 2-km ADAS wind speed and wind vectors at 480 m. Wind speed is contoured every 2 m s^{-1}, shaded above 6 m s^{-1}, while wind vectors are denoted by arrows. Valid times are (a) 2215, (b) 2230, (c) 2245, and (d) 2300 UTC 26 Jul 1997. The SW–NE line denotes the cross section shown in Fig. 4.

the vertical correlation range for surface and radar observations, the outflow boundary could be analyzed as a single continuous feature from the surface to 1000 m, in advance of the midlevel wind maximum (1000–3000 m) associated with the dissipating thunderstorm.

The evolution of the thunderstorm outflow can also be examined through the divergence of the horizontal wind on the 2-km analysis grid. In Fig. 5, plots of convergence (shaded), divergence (dashed lines), and horizontal winds are shown at 650 m. At 2215 UTC, an area of convergence is found over much of central Brevard County along the leading edge of the developing outflow boundary (Fig. 5a). Weak divergence is also found over northeastern Osceola County at this time. Fifteen minutes later, an extensive area of low-level divergence develops in southern Brevard County, behind the significant outflow boundary (Fig. 5b). Convergence along the outflow boundary spreads outward into central Brevard County (just south of KSC/CCAFS), offshore of southern Brevard County, and into Indian River County. Divergence continues to intensify across much of interior Brevard County over the next 30 min beneath

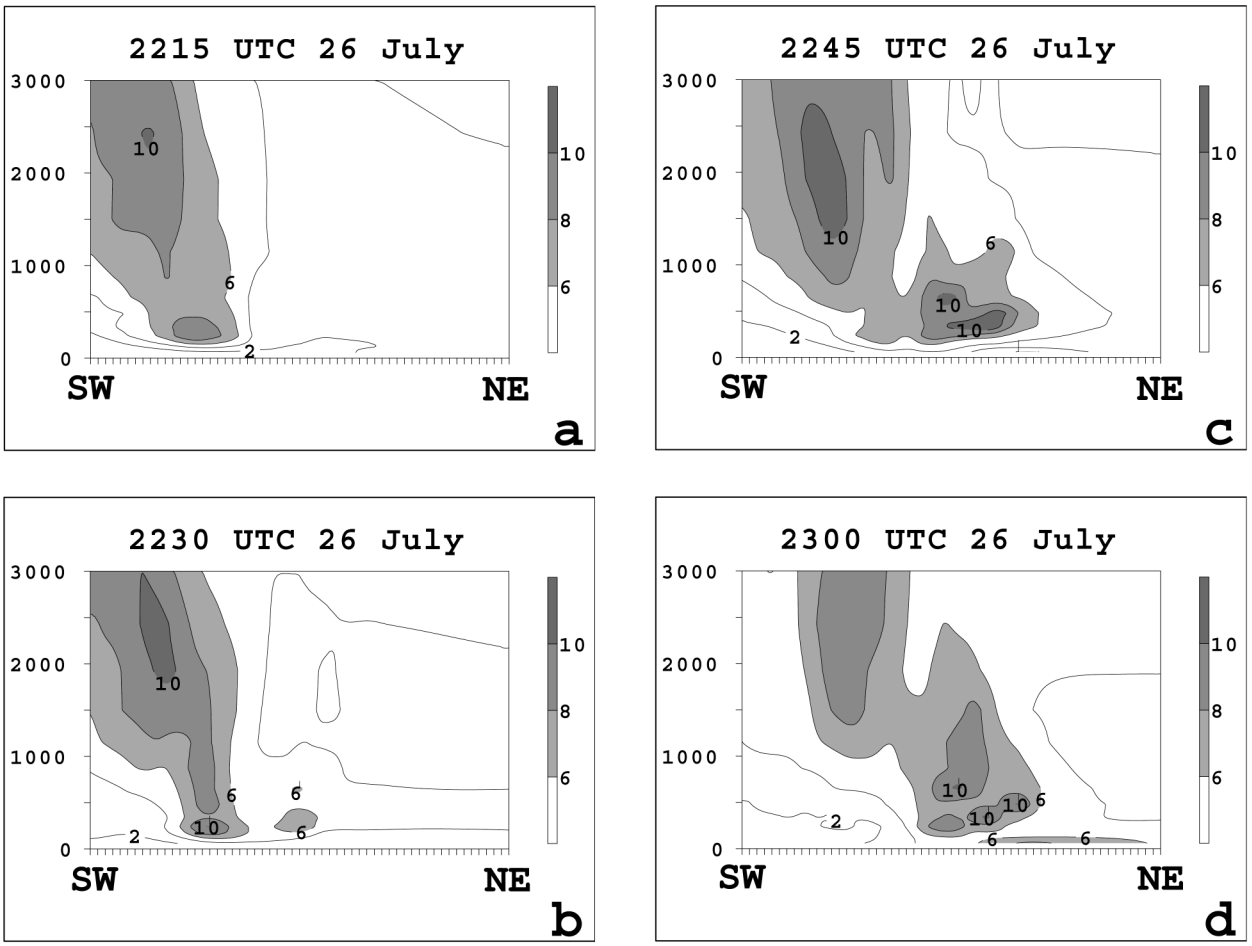

FIG. 4. A SW–NE cross section of wind speeds on the 2-km analysis grid with winds >6 m s^{-1} shaded according to the scale provided. The orientation of the cross section is denoted in Fig. 3. Valid times are (a) 2215, (b) 2230, (c) 2245, and (d) 2300 UTC 26 Jul 1997. The vertical axis extends from the surface to 3000 m.

the dissipating thunderstorm (Figs. 5c,d), while the band of convergence spreads out radially along the leading edge of the outflow boundary. Notice that the divergence pattern is somewhat radial in nature due to the strong dependence of the analysis on WSR-88D data in this case. The resulting constant-height analyses are comparable to examining a WSR-88D constant altitude plan position indicator, a product that is not available in the current suite of real-time WSR-88D products.

By 2300 UTC, a well-defined band of convergence arcs from northern Osceola County, across eastern Orange and northern Brevard Counties, into the offshore waters of Brevard County, and then back onshore in Indian River County (Fig. 5d). Strong divergence exceeding 8×10^{-4} s^{-1} occurs over east-central Brevard County. A cross section through this maximum in low-level divergence at 2300 UTC reveals some interesting structure as shown in Fig. 6. A large area of strong midlevel convergence is depicted above the low-level divergence maximum in the center of Fig. 6a. The low-level convergence associated with the outflow boundary is also seen on the far left and far right of Fig. 6a between the surface and 1000 m. In Fig. 6b, the vertical velocity field[1] reveals significant sinking motion exceeding -150 cm s^{-1} between 2250 and 5750 m above the low-level divergence field shown in Fig. 6a. The structure of this circulation depicts the consistency between the strong mesoscale subsidence above the ground and the lateral spreading of the horizontal winds associated with the outflow boundary near the surface (Fig. 6b). Forecasters could examine these vertical velocity fields in conjunction with the horizontal winds to gain insight into the current mesoscale properties of the convective system. In addition, it is imperative to initialize short-range NWP models with an analysis containing such 3D structure in order to capture the existence, development, and maintenance of active

[1] In ADAS, vertical velocities are derived by integrating the continuity equation using the horizontal winds at all vertical levels and top and bottom boundary conditions ($w = 0$ at boundaries). The horizontal wind field is then adjusted/relaxed in order to conserve total mass divergence (Brewster 1996).

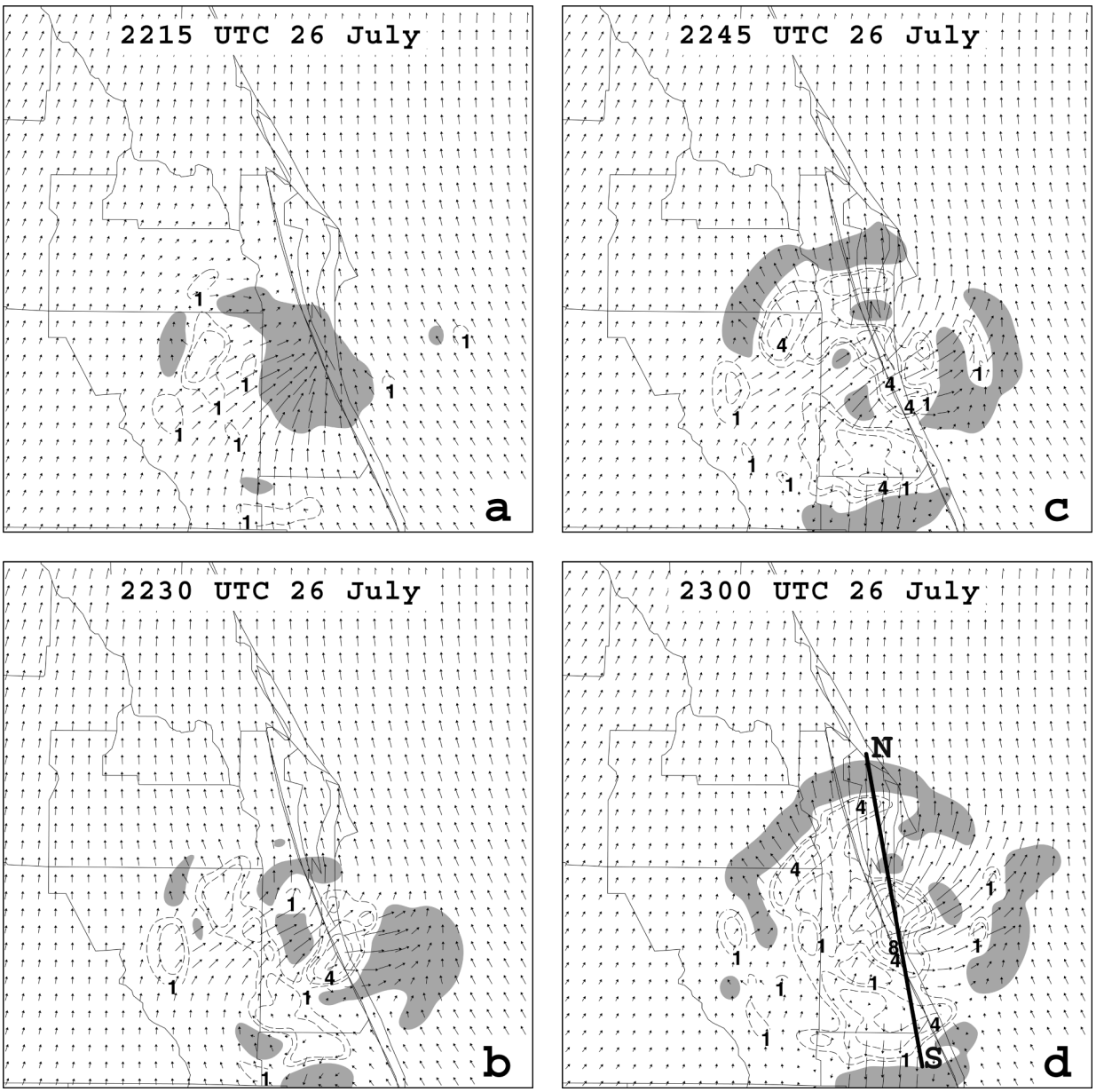

FIG. 5. Divergence of the horizontal wind ($\times 10^{-4}$ s^{-1}) and wind vectors at 650 m derived from the 2-km analysis grids. Dashed lines indicate divergence and shading indicates convergence. Valid times are (a) 2215, (b) 2230, (c) 2245, and (d) 2300 UTC 26 Jul 1997. (d) The N–S line denotes the cross section shown in Fig. 6.

convection after initiation. These analyses could subsequently serve to initialize a short-range, local NWP model when such a model is implemented at SMG and the NWS MLB.

The ability to analyze convection and its associated outflow in this manner demonstrates the potential value of this ADAS configuration. It is noticeably easier to diagnose and visualize the outflow boundary using ADAS analyses rather than radial velocity radar data at multiple elevation angles. Operational forecasters supporting this Atlas launch could have used this sequence of ADAS analyses to interpret quickly the increasing risk of winds exceeding the vehicle's allowable limits by analyzing graphical products such as those shown in Figs. 3 through 6. Furthermore, these wind products would be helpful to NWS MLB meteorologists when forecasting additional convection along outflow boundaries or relaying information about sudden wind shifts to local wildfire agencies. Such analysis products may help the forecaster to diagnose more efficiently the structure and evolution of outflow boundaries like the one from 26 July 1997.

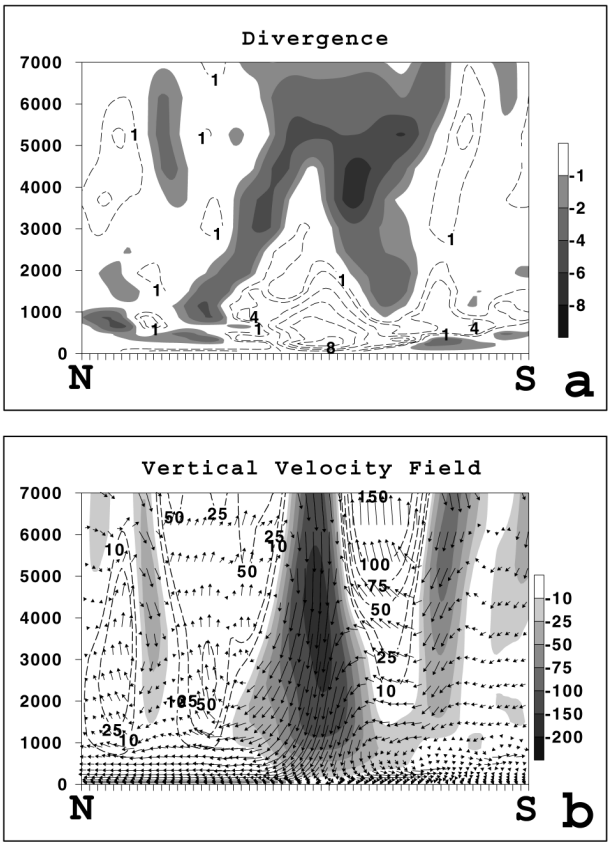

FIG. 6. Cross section of (a) divergence and (b) vertical velocity/circulation (derived from the 2-km analysis grids) at 2300 UTC 26 Jul 1997 along the line indicated in Fig. 5d. (a) Dashed lines denote divergence of the horizontal wind field and convergence is shaded according to the scale. (b) Vertical velocity (cm s^{-1}) and the sense of the vertical circulation are given by arrows. The vertical axis ranges from 0–7000 m in both panels. Rising motion is indicated by dashed contours while shading represents sinking motion according to the scale provided. Vertical velocities are scaled by a factor of 100 to depict circulation in the plane of the cross section.

b. 28 February 1999 case study: Prefrontal squall line

This particular case was chosen because space launch and landing rules pertaining to lightning, thick clouds, and ceilings were all violated on this day. The derived cloud-top and ceiling heights are shown in order to illustrate how ADAS may be used in real time to diagnose qualitatively and quantitatively the cloud properties associated with the convective line.

A strong southwest flow of warm, relatively moist air occurred ahead of a southeastward-moving surface cold front on this day. Temperatures reached the mid to upper 20°C range whereas dewpoint temperatures were in the mid 10°C range across east-central Florida ahead of a prefrontal line of thunderstorms. The maximum convective available potential energy (CAPE; 1200–1600 J kg^{-1}) and minimum lifted indices (−5° to −6°C) occurred along the west coast of Florida where surface dewpoint temperatures approached 20°C. Over east-central Florida, the maximum CAPE was less than 1200 J kg^{-1} throughout the event. Wind speeds were strong throughout the troposphere including 10 m s^{-1} at the surface, 15 m s^{-1} at 850 mb, 25 m s^{-1} at 500 mb, and over 50 m s^{-1} at 300 mb. Winds veered with height from south-southwesterly at the surface to westerly at 500 and 300 mb. The combination of strong vertical wind shear and moderate instability resulted in the development of a few strong to severe thunderstorms on this day.

Base reflectivity data from WSR-88D depicting the prefrontal line of thunderstorms is shown every half-hour from 1813 to 2044 UTC 28 February (Fig. 7). A southwest–northeast line of thunderstorms moved southeastward between 1813 and 1913 UTC (Figs. 7a–c) approaching the northern portions of KSC/CCAFS by 1913 UTC. A particularly intense cell embedded in this line (labeled as #1), with reflectivities approaching 55 dB*Z*, pushed offshore to the north of KSC/CCAFS. At about 1943 UTC, two distinct cells developed to the southwest of KSC/CCAFS (labeled #2 and #3 in Fig. 7) and moved eastward through 2014 UTC (Figs. 7d–e). The broken line of convection continued to propagate southeastward and moved offshore to the east of KSC/CCAFS and MLB by 2044 UTC (Fig. 7f).

The CCS of ADAS can serve as a tool for diagnosing the quantitative properties of clouds. The cloud products empirically derived in ADAS provide the means for quickly assessing various quantitative properties of clouds such as ceilings, cloud-top heights, and cloud thicknesses, as compared to examining individual *GOES-8* images, surface reports, and multiple WSR-88D data products.

The 2-km derived cloud-top and ceiling heights are given in Figs. 8 and 9, respectively, and correspond to the times in the base reflectivity images of Fig. 7. The anvils associated with the individual thunderstorms are clearly depicted in the sequence of cloud-top heights (Fig. 8). In particular, note the high cloud tops exceeding 12.5 km to the north and northeast of KSC/CCAFS associated with cell #1 (labeled in Figs. 7a,b and Figs. 8a,b). The horizontal extent of the anvil associated with the squall line is illustrated by the nearly continuous band of high cloud-top heights in Figs. 8a–c (>7.5 km). As the squall line begins to break apart (Fig. 7d), the single area of cloud-top heights greater than 7.5 km split into two distinct areas to the southwest of KSC/CCAFS (Fig. 8d). Finally, the anvils of two distinct areas of convection are depicted by cloud-top heights exceeding 7.5 km at 2015 and 2045 UTC (Figs. 8e,f). These regions are labeled as cells #2 and #3 in Figs. 7d–f and Figs. 8d–f, respectively. These cloud-top height fields could be used by SMG and 45 WS forecasters when evaluating various LCC and FR.

The derived ceiling heights are shown in Fig. 9 for the same times as in Fig. 8. High cloud ceilings are analyzed at 1815 UTC, especially along the leading edge of the squall line where ceiling heights exceed 5 km in

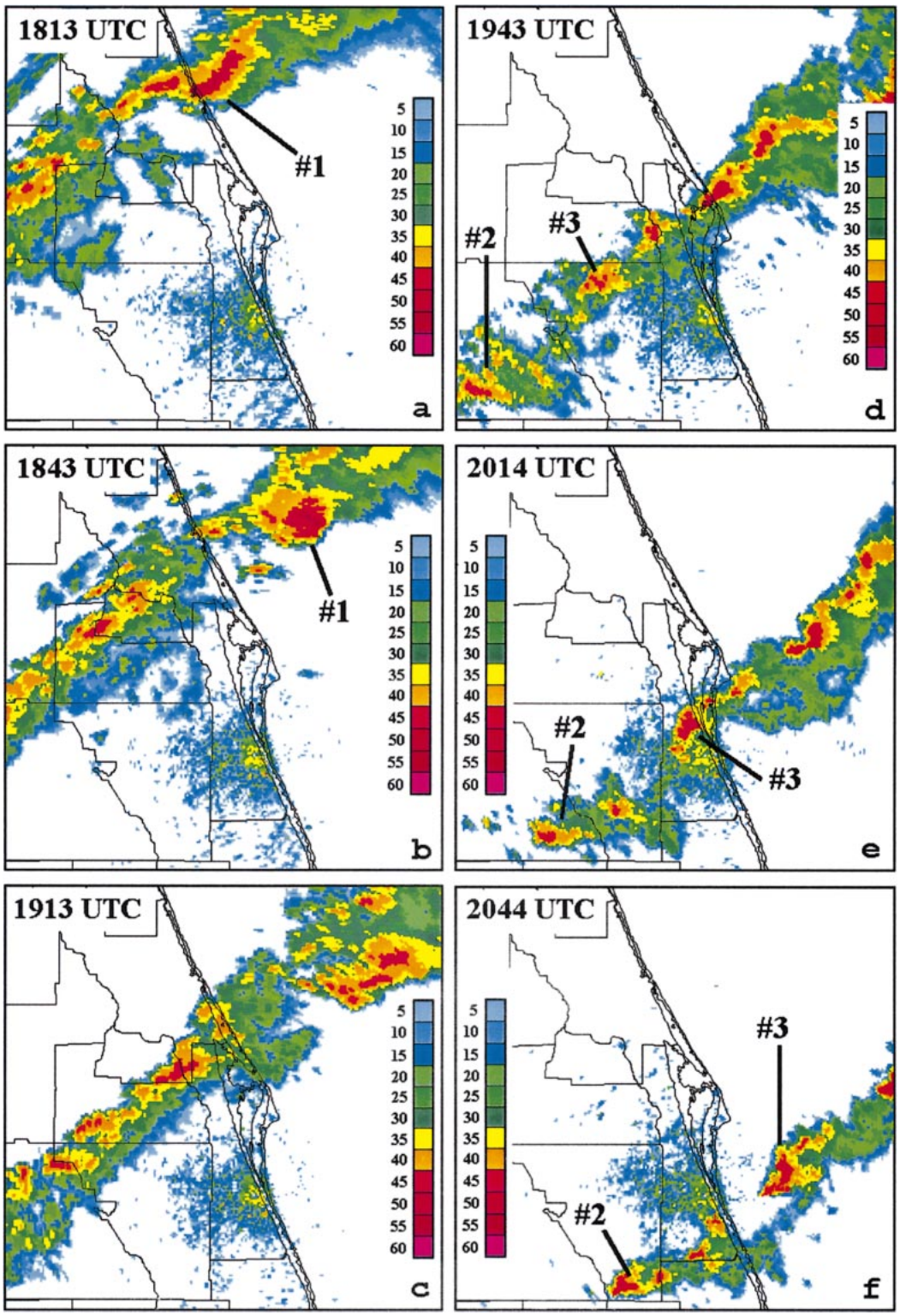

FIG. 7. Base reflectivity images (elevation angle of 0.5°) from the MLB WSR-88D are shown over east-central Florida from 28 Feb 1999 at the following times: (a) 1813, (b) 1843, (c) 1913, (d) 1943, (e) 2014, and (f) 2044 UTC. Here, #1, #2, and #3 denote three specific cells described in the text.

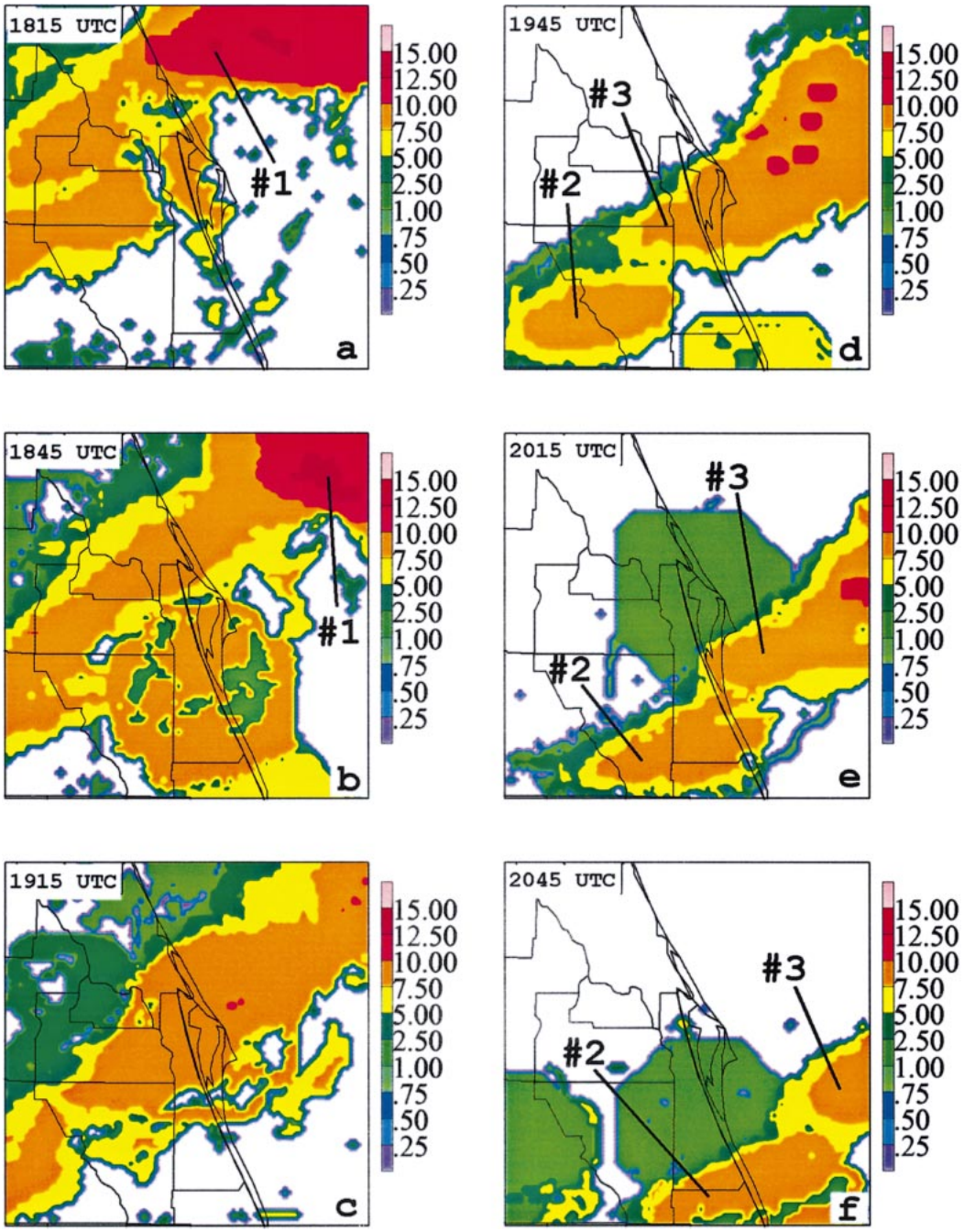

FIG. 8. ADAS 2-km cloud-top heights (km) are depicted according to the scale on the right-hand side of each panel. Valid times are for 28 Feb 1999 at (a) 1815, (b) 1845, (c) 1915, (d) 1945, (e) 2015, and (f) 2045 UTC. Here, #1, #2, and #3 denote the anvils associated with the three specific cells described in the text.

the vicinity of the thunderstorm anvil (Fig. 9a). Ceiling heights decrease to 250–500 m by 1845 UTC to the northwest of KSC/CCAFS, whereas higher ceiling heights are diagnosed over the ocean northeast of KSC/CCAFS (Fig. 9b). In Figs. 9c–d, the highest ceilings continue along the leading edge of the line of storms while lower ceilings associated with the precipitation occur towards the back edge of the line of thunderstorms. Very low ceilings (less than 50 m in some locations) associated with a severe thunderstorm are analyzed in the vicinity of Patrick Air Force Base (COF) at 2015 UTC (Fig. 9e). The areal coverage of analyzed ceilings decreases as the storms continue moving southeastward by 2045 UTC (Fig. 9f).

SMG forecasters could use these ADAS-analyzed cloud ceiling heights to monitor the evolution of cloud

ceilings less than 2438 m (8000 ft) during space shuttle landing operations. In addition, NWS MLB forecasters could use this analyzed cloud information when composing TAF. The potential utility of these cloud ceiling products is that the areal extent of ceilings less than the critical thresholds for Shuttle landings or TAF criteria can be clearly depicted in graphical displays similar to that shown in Fig. 9. By animating multiple cloud analysis products, the forecaster could obtain a better understanding of the horizontal and temporal variations in cloud ceilings in a shorter amount of time compared to examining multiple surface observations from several different METAR stations.

6. Sensitivity of analyses to observational data

This section discusses some of the problems and deficiencies that were encountered during the real-time simulation of ADAS. The temporal discontinuities in the analyzed cloud products and some possible solutions to this problem are discussed. In addition, comparisons are made between the influence of Level II versus Level III WSR-88D data on the subsequent analyses. The deficiencies of the system as a result of using Level III WSR-88D data are examined and the improved analysis fields are shown when utilizing the full-volume Level II data.

a. Temporal discontinuity of cloud products

The continuity of the analyzed cloud fields in this particular configuration of ADAS are highly dependent on the available data that are integrated. The transition of ceiling heights in Figs. 9d–e provides a good example of how the availability of observational data influences the continuity of the cloud analyses. The severe thunderstorm that moved through COF originated over eastern Osceola County at 1945 UTC (Fig. 9d) where no surface METAR observations of clouds are available. When the cell moved into the vicinity of the COF METAR station, the combination of a special COF observation and all other available data generated the very low ceiling analysis at 2015 UTC (Fig. 9e). This sequence of cloud analyses does not necessarily suggest that the ceiling suddenly decreased between 1945 and 2015 UTC. In this instance, no METAR cloud observations were available at 1945 UTC to provide a report of low ceilings, resulting in the sharp transition of ceiling heights shown in Figs. 9d–e. Analyses of cloud characteristics such as ceiling heights could be improved in ADAS by incorporating satellite cloud classification data with surface cloud-base reports (Forsythe et al. 2000). In addition, better temporal continuity of the cloud fields could be achieved by running ADAS in a cycling mode with the ARPS NWP model.

b. Impact of Level II versus Level III WSR-88D data

The comparison between ADAS analyses using Level II versus Level III data was conducted on the 28 February 1999 case because this day contained the greatest number of radar returns from the simulated real-time ADAS trial period. The control run used Level III WSR-88D data from all Florida radar sites. The analysis programs were then rerun for a 9-h period (1500–2345 UTC) using Level II data from only the MLB WSR-88D. Because the 2-km analysis grid contains radar data primarily from the MLB WSR-88D, all comparisons are made on the 2-km grid only, thereby isolating as much as possible the differences purely due to Level II versus Level III WSR-88D data, rather than the influence of surrounding radars.

As described in section 4d, insufficient coverage or large variance of reflectivity or radial velocity within an individual grid volume results in rejection of data at a particular location on the analysis grid. Three factors lead to fewer remapped reflectivity and radial velocity grid volumes using Level III data compared to Level II data. First, because Level II data contain all 14 elevation angles of data at a finer horizontal resolution compared to Level III data, the volumetric coverage at a particular location on the analysis grid is more substantial using Level II data. Second, more Level II data are available at upper levels due to the higher elevation angles. Third, Level III data experience larger variances because of the categorization of reflectivity and radial velocity into discrete bins (Table 4). Also note that due to this categorization, a larger error variance is assigned to the Level III radial velocity data, which effectively lowers the weight applied to these data compared to Level II data.

Figure 10 illustrates the number of remapped radial velocity grid volumes on the 2-km analysis grid for both Level II and Level III WSR-88D data at each analysis time within the 9-h comparison window. Between 1800 and 2100 UTC, the number of remapped radial velocity grid volumes on the 2-km grid using Level II data greatly exceeds the number of radial velocity observations using Level III data. The maximum number of remapped radial velocity grid volumes is 7968 for Level III data at 1930 UTC and 19 631 for Level II data at 1945 UTC (Fig. 10). A secondary maximum of remapped Level III radial velocity grid volumes occurs at 1800 UTC but is not prevalent in the Level II data. This secondary peak results from TBW and JAX Level III data that are remapped onto the 2-km analysis grid in addition to the MLB Level III data.

A consequence of the increased number of remapped radial velocity data associated with Level II data is the ability to detect more subtle boundaries and wind shift lines. This statement is supported by a diagnosis of the low-level cold frontal passage and its associated wind shift line using ADAS analyses ingesting Level II versus Level III WSR-88D data. The prefrontal line of thunderstorms examined in section 4 propagated through KSC/CCAFS between 1900 and 2000 UTC 28 February 1999. The low-level cold front moved through KSC/CCAFS at about 2200 UTC accompanied by a wind

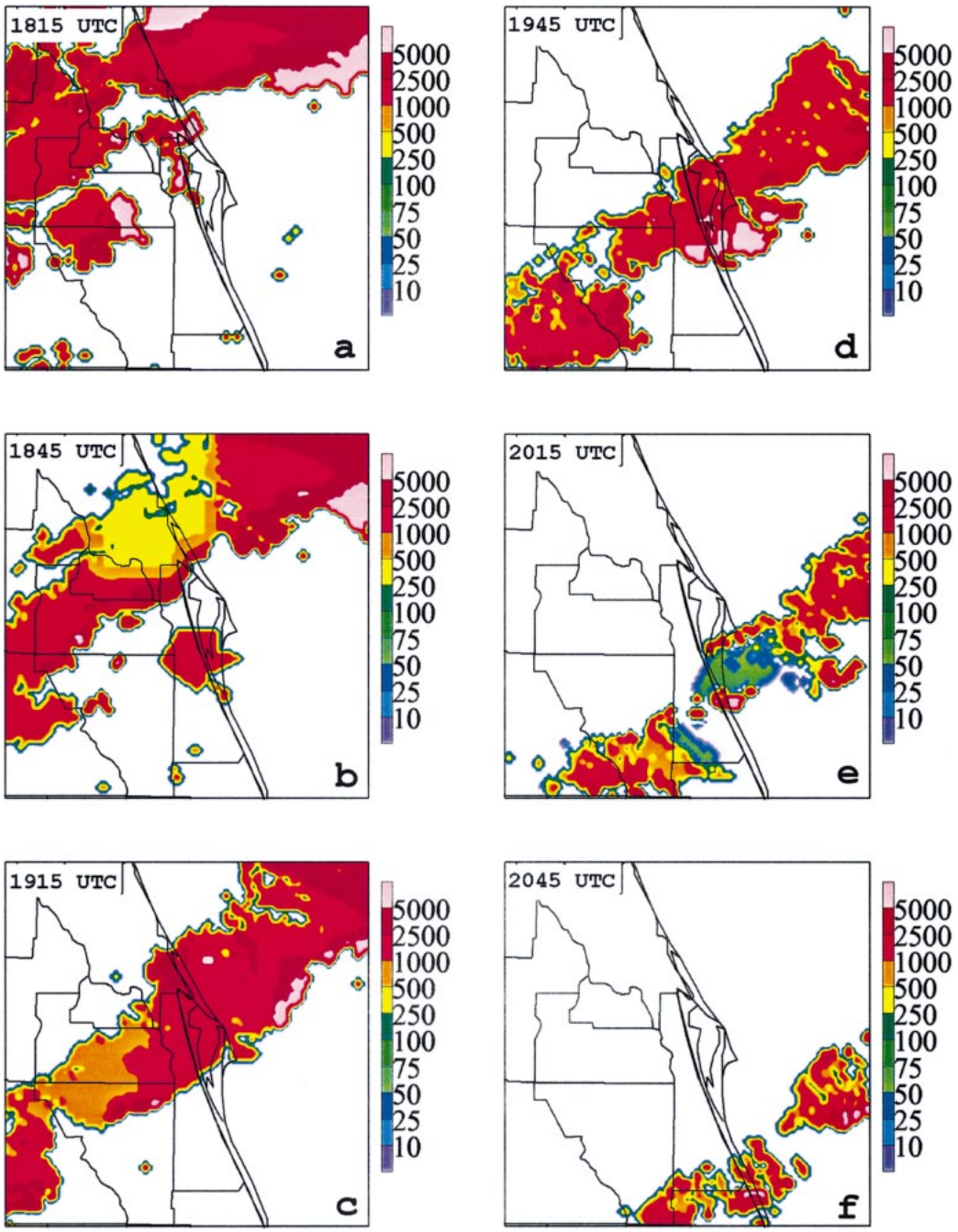

FIG. 9. ADAS 2-km ceiling heights (m) are depicted according to the scale on the right-hand side of each panel. Valid times are for 28 Feb 1999 at (a) 1815, (b) 1845, (c) 1915, (d) 1945, (e) 2015, and (f) 2045 UTC.

shift from southwest to west and no significant weather features (not shown).

Divergence plots at 870 m using Level III data illustrate to a limited extent the areas of low-level convergence/divergence associated with the individual thunderstorms. At 2015 UTC, when a severe thunderstorm propagated through central Brevard County, a region of low-level convergence is depicted in the vicinity of the severe convection (Fig. 11a, corresponding to the reflectivity in Fig. 7e). Between 2030 and 2100 UTC, small couplets of convergence and divergence are associated with the southeastward-moving line of convection (Figs. 11b and 12a,b).

Many more details of the convection and frontal movement are revealed by the analyses using Level II WSR-88D data. The convergence associated with the

TABLE 4. Categorization of Level III reflectivity and radial velocity product data into assigned bins.

Mode	Reflectivity	Radial velocity
Precipitation	16 levels: 0–75 dBZ, every 5 dBZ; 1 missing data level	16 levels: −64, −50, −36, −26, −16, −10, −1, 0, 10, 16, 26, 36, 50, 64 kt 1 missing data level 1 range folding
Clear air	16 levels: −28 to + 28 dBZ, every 4 dBZ; 1 missing data level	Same as above

severe cell and nearby convection at 2015 UTC shows much more structure when using Level II WSR-88D data (Fig. 11c). Beginning at 2030 UTC, a linear band of convergence develops to the northwest of KSC/CCAFS with the approach of the cold frontal zone (Fig. 11d). This banded feature propagates slowly southeastward over the next 30 min reaching northern KSC/CCAFS by 2100 UTC (Figs. 12c–d). The benefits of using Level II WSR-88D data are quite obvious. Ingesting Level II data allows ADAS to generate more detail with regards to the wind features and areas of convergence associated with convection and the cold-frontal wind shift. The benefits of using Level II data can be even more important during the Florida warm season when interactions between multiple thunderstorm outflow boundaries frequently occur (Wilson and Megenhardt 1997).

Despite the greater volume of Level II versus Level III WSR-88D data, the impact of Level II data on the cloud and moisture fields is rather insignificant on 28 February. This fact is illustrated through time–height cross sections of cloud liquid, cloud ice, and relative humidity fields at the Shuttle Landing Facility (TTS) using Level II versus Level III data. The cloudiness associated with the passage of the prefrontal line of convection is depicted in Figs. 13a and 13c using Level III and Level II WSR-88D data, respectively. With Level III data, the derived cloud liquid field extends from the surface to 350 mb, whereas cloud ice extends from 550 to above 250 mb between 1900 and 2000 UTC 28 February (Fig. 13a). Qualitatively, the derived cloud fields using Level II data are very similar to the fields using Level III data except that the cloud concentrations are slightly greater and the cloud liquid field extends to a higher level (~275 mb; Fig. 13c). The relative humidity fields using Level III versus Level II data (shaded regions in Figs. 13b and 13d respectively) are also nearly identical.

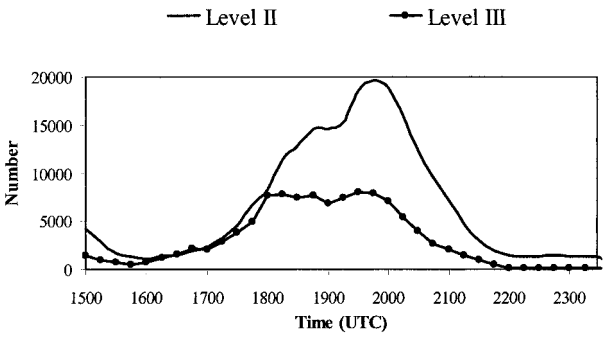

FIG. 10. A plot of the number of radial velocity points remapped onto the 2-km analysis grid is given every 15 min on 28 Feb 1999 using all six Florida Level III WSR-88D sites (line with data points) and Level II data for the MLB WSR-88D site only (solid line).

Since Level II data have a greater influence on the horizontal winds than Level III data, the impact on the vertical velocity field is more significant. The differences in the derived vertical velocity fields using Level III versus Level II data are shown in Figs. 13b and 13d. At 1930 UTC, a deep area of rising motion associated with the squall line passage (maximum > 30 cm s^{-1}) is analyzed between 850 and 250 mb using Level III data (Fig. 13b). However, the same time–height cross section using Level II data reveals a much more intense updraft between 850 and 350 mb (maximum > 75 cm s^{-1}) as well as a downdraft on the trailing edge of the squall line (Fig. 13d). Sinking motion exceeds -100 cm s^{-1} in the mid to upper troposphere at 1945 UTC and extends down to near the surface at a lesser magnitude by 2000 UTC (dashed contours in Fig. 13d). Operationally, it is important to be able to diagnose regions of strong subsidence associated with convective activity because this sinking motion can lead to strong low-level horizontal winds as observed in this particular case.

This example shows the importance of analyzing real-time Level II rather than Level III WSR-88D reflectivity and radial velocity data to obtain the highest quality analysis products. This experiment has implications to operational forecast centers using AWIPS since it currently ingests only Level III WSR-88D data for display and input to local 3D LAPS analyses. To acquire Level II data for ADAS, the NWS MLB uses software from the Collaborative Radar Acquisition Field Test (CRAFT; Droegemeier et al. 1999), which compresses and transmits Level II data in real time. The CRAFT software enables the NWS MLB to process and ingest Level II data for ADAS, as well as transfer the compressed files via the Internet to SMG (and other locations), all in real time.

7. Summary and future direction

This paper describes the AMU's work in configuring ADAS for the operational needs of east-central Florida.

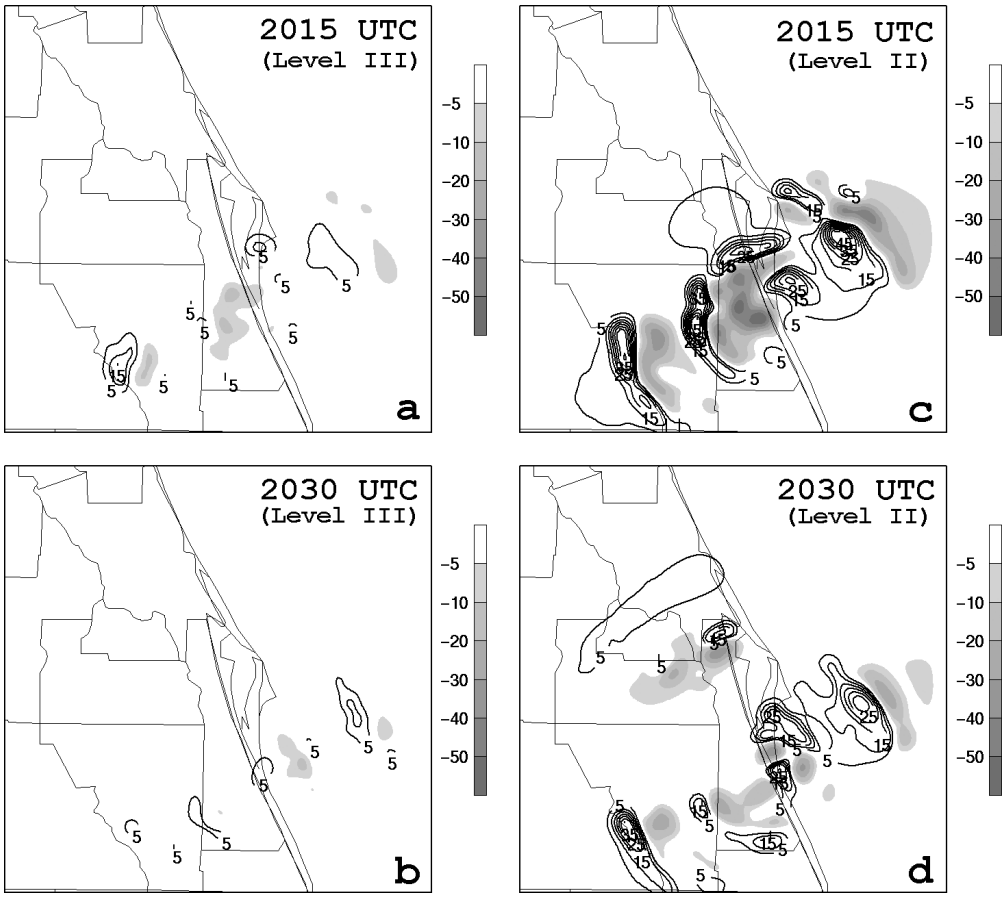

FIG. 11. Plots of ADAS 2-km divergence ($\times 10^{-5}$ s^{-1}) at 870 m are compared using (a), (b) Level III WSR-88D data, and (c), (d) Level II WSR-88D data. Shading represents convergence according to the scale provided whereas solid contours denote divergence. Valid times on 28 Feb 1999 are (a), (c) 2015 UTC, and (b), (d) 2030 UTC.

The ultimate goal for running ADAS in east-central Florida is to generate real-time graphical products that may enhance weather nowcasts and short-range (<6 h) forecasts issued by the 45 WS, SMG, and NWS MLB. During the course of the project, the AMU determined the potential utility of ADAS for east-central Florida, simulated a real-time ADAS configuration, and implemented a real-time version of ADAS at both SMG and the NWS MLB. This paper presented sample analysis products from a simulated real-time ADAS during complex, operationally significant weather situations.

A real-time ADAS configuration can provide added value for nowcasts and short-term forecasts because it integrates all operationally available data in east-central Florida and it is run at fine spatial and temporal resolutions. In combination with a visualization tool such as GEMPAK or AWIPS, this real-time ADAS configuration can provide forecasters with the means to develop a more comprehensive understanding of evolving fine-scale weather features than could be developed by individually examining the raw meteorological data sources.

ADAS was configured to generate high-resolution analyses in space and time on grids with horizontal resolutions of 10 km and 2 km. It was shown that by examining sequences of high-resolution ADAS analyses, fine-scale features such as outflow boundaries can be conceptualized quite easily by forecasters. In addition, the trends of cloud features such as ceilings and cloud-top heights provided by the ADAS CCS could be used by forecasters to monitor FR, LCC, and TAF thresholds in support of space missions and general aviation forecasting.

This paper also compared analyses ingesting Level II versus Level III WSR-88D data. In general, the quality and amount of remapped Level II radar observations greatly exceeds the Level III radar observations. As a result, analyses using Level II WSR-88D data can portray wind shift lines and vertical circulations more adequately. An advantage of using Level III WSR-88D data is that data can be received from all Florida radar sites resulting in increased horizontal coverage of radar data at low levels.

From 2000–2001, the AMU assisted both SMG and NWS MLB in installing and configuring a real-time version of ADAS at each office. SMG began running ADAS in real time during July 2000 whereas the real-

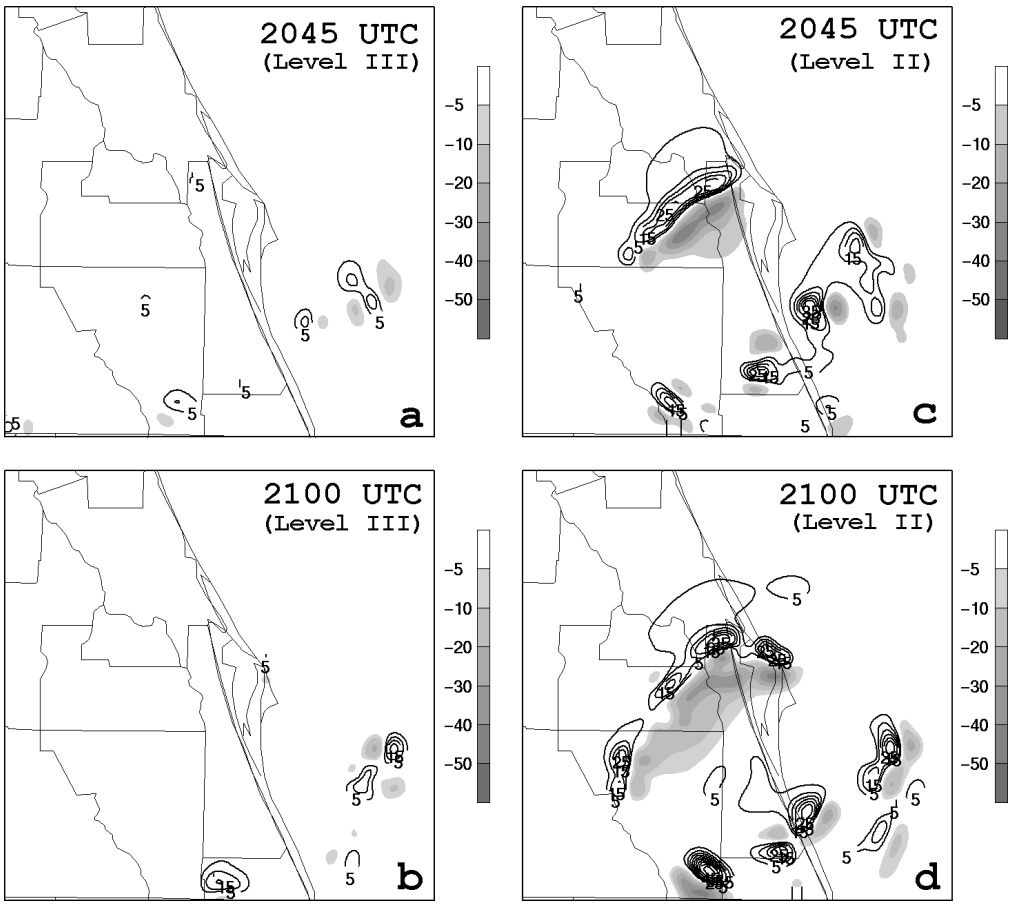

FIG. 12. Plots of ADAS 2-km divergence ($\times 10^{-5}$ s^{-1}) at 870 m are compared using (a), (b) Level III WSR-88D data, and (c), (d) Level II WSR-88D data. Shading represents convergence according to the scale provided whereas solid contours denote divergence. Valid times on 28 Feb 1999 are (a), (c) 2045 UTC, and (b), (d) 2100 UTC.

time ADAS at the NWS MLB was completed in April 2001. An important goal is to incorporate the ADAS analyses into AWIPS at both SMG and the NWS MLB in order to take advantage of the suite of display utilities and functions available in AWIPS. The long-term goal includes running ADAS in conjunction with a locally configured NWP model.

The utility of real-time high-resolution grid analyses can extend beyond just an analysis tool by serving as an initialization to high-resolution local NWP models. As NWP models are run locally at finer grid spacing for specific applications, care must be exercised to properly initialize the models by preserving the fine-scale details of meso- and convective-scale phenomena. A utility such as the ADAS described in this paper can provide the initial conditions necessary to capture and preserve these fine-scale details in an analysis-forecast cycle. In such a configuration, these analyses can be used to initialize a local NWP model at high temporal frequencies, whereas the short-range NWP forecasts can provide the background fields for subsequent analyses. This type of scheme could preserve and better forecast features such as thunderstorm outflow boundaries. Additional techniques such as dual-Doppler and thermodynamic retrievals (Lin et al. 1993; Sun and Crook 1996; Shapiro and Mewes 1999) and four-dimensional data assimilation methods (Hoke and Anthes 1976; Bloom et al. 1996), combined with high-resolution analyses, have the potential to provide extensive added value to local numerical weather forecasting. Therefore, the ultimate goal is to utilize such tools and capabilities to provide a locally configured, high-resolution numerical analysis and prediction system to meteorologists supporting east-central Florida operational weather forecasting.

Acknowledgments. The authors would like to thank Mr. Johnny Weems of the 45th Weather Squadron for supplying data and information about the Atlas launch mission. The authors also thank Dr. Frank Merceret and Mr. Bill Roeder for their constructive comments on earlier versions of the manuscript. In addition, we thank Drs. Kelvin Droegemeier, Keith Brewster, and Jian Zhang for their extensive guidance, support, and suggestions in configuring the ADAS software for this application. Finally, the authors greatly appreciate the con-

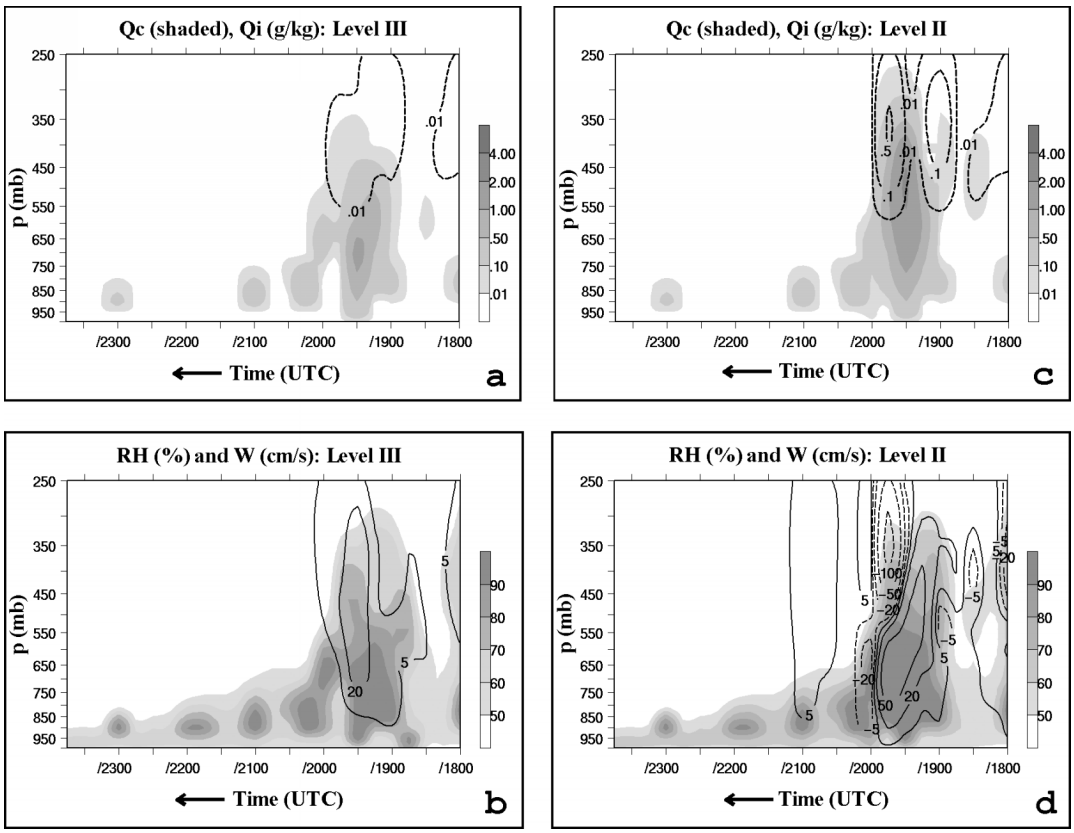

FIG. 13. Time–height cross sections at TTS illustrating the influence of Level II vs Level III WSR-88D data are displayed from 1800 to 2345 UTC 28 Feb 1999. Derived cloud liquid (q_c, $\times 10^{-3}$ g kg^{-1}, shaded according to the scale provided) and cloud ice (q_i, contoured, $\times 10^{-3}$ g kg^{-1}) mixing ratio fields are shown using (a) Level III WSR-88D data and (c) Level II WSR-88D data. Derived relative humidity (RH, shaded in % according to the scale provided) and vertical velocity (cm s^{-1}, dashed contours indicate negative values or sinking motion) fields are shown using (b) Level III WSR-88D data and (d) Level II WSR-88D data.

structive comments from three anonymous reviewers who helped to improve dramatically the quality and focus of the paper.

Mention of a copyrighted, trademarked, or proprietary product, service, or document does not constitute endorsement thereof by the authors, ENSCO, Inc., the AMU, the National Aeronautics and Space Administration, or the United States Government. Any such mention is solely for the purpose of fully informing the reader of the resources used to conduct the work reported herein.

APPENDIX

The Bratseth Technique and ADAS Multipass Configuration

In the Bratseth objective analysis technique as utilized by ADAS, a variable s is analyzed at grid point x using observations s_j. For the nth iteration or pass,

$$s_x(n) = s_x(n-1) + \sum_{j=1}^{N} \alpha_{xj}[s_j^o - s_j(n-1)], \quad \text{(A1)}$$

where the analysis at the observation location is given by

$$s_j(n) = s_j(n-1) + \sum_{k=1}^{N} \alpha_{jk}[s_k^o - s_k(n-1)], \quad \text{(A2)}$$

and N is the total number of observations. In Eqs. (A1) and (A2), the weights applied to each observation are given by

$$\alpha_{xj} = \frac{\rho_{xj}}{m_j}, \quad \text{and} \quad \text{(A3)}$$

$$\alpha_{jk} = \frac{(\rho_{jk} + \epsilon^2 \delta_{jk})}{m_j}, \quad \text{(A4)}$$

where ϵ^2 is the ratio of the observational error variance to the background error variance, and δ_{jk} is the Kronecker delta function, which is unity when $j = k$ and zero when $j \neq k$.

Within the weights of Eqs. (A3) and (A4) are correlation functions (ρ_{xj} and ρ_{jk}) that are modeled as Gaussian and assume a separation between the horizontal and vertical scales:

TABLE A1. A list of the objective analysis parameters for the simulated real-time ADAS configuration, consisting of the horizontal (L_h, km) and vertical correlation ranges (L_v, m) and data usage for each pass for both the 10-km and 2-km grids.

	10-km analysis			2-km analysis		
Pass #	L_h (km)	L_v (m)	Data used	L_h (km)	L_v (m)	Data used
1	150	250	Air, raob	30	250	Air, raob
2	100	20	Sfc	20	20	Sfc
3	50	20	Tower, prof	10	20	Tower, prof
4	20	100	Radar	4	100	Radar

Air = ACARS + pilot reports.
Sfc = METAR + buoy/ship.
Tower = KSC/CCAFS towers.
Radar = Level III WSR-88D products for all Florida radar sites (JAX, BYX, AMX, MLB, TLH, TBW).
Prof = 915-MHz and 50-MHz KSC/CCAFS profilers.
Raob = Rawinsonde for XMR only.

$$\rho_{xj} = \exp\left(\frac{-|r_{xj}|^2}{L_h^2}\right)\exp\left(\frac{-|\Delta z_{xj}|^2}{L_v^2}\right) \quad \text{(A5)}$$

$$\rho_{jk} = \exp\left(\frac{-|r_{jk}|^2}{L_h^2}\right)\exp\left(\frac{-|\Delta z_{jk}|^2}{L_v^2}\right). \quad \text{(A6)}$$

In Eqs. (A5) and (A6), r_{xj} and Δz_{xj} are the horizontal and vertical distances between the grid point and an observation, r_{jk} and Δz_{jk} are the horizontal and vertical distances between successive observations, and L_h and L_v represent the user-specified horizontal and vertical (e-folding) influence ranges, respectively. Finally, the weights in Eqs. (A3) and (A4) are normalized by the data density surrounding each observation, given by

$$m_j = \epsilon^2 + \sum_{k=1}^{N} \rho_{jk}. \quad \text{(A7)}$$

A summary of the number of objective analysis passes, the user-specified influence ranges, and the data used for each pass is provided in Table A1. The influence ranges L_h and L_v are carefully chosen for each data source in order to retain observational features and to prevent data from influencing too much (or too little) of the analysis grid. Data with a fine (coarse) horizontal resolution are assigned a small (large) L_h in order to preserve the resolvable features of the data source. In addition, a small L_v is used for data with fine vertical resolution (e.g., KSC/CCAFS profilers and wind towers) and for data that should have a limited vertical influence (e.g., surface observations). An observation located at a horizontal (vertical) distance L_h (L_v) from a grid point receives a weight of e^{-1}. At larger (smaller) distances, observations receive less (more) weight.

REFERENCES

Albers, S. C., 1995: The LAPS wind analysis. *Wea. Forecasting,* **10,** 342–352.

——, J. A. McGinley, D. A. Birkenheuer, and J. R. Smart, 1996: The local analysis and prediction system (LAPS): Analysis of clouds, precipitation, and temperature. *Wea. Forecasting,* **11,** 273–287.

Barnes, S. L., 1964: A technique for maximizing details in numerical weather map analysis. *J. Appl. Meteor.,* **3,** 396–409.

Benjamin, S., and K. Brundage, cited 2001: RUC/MAPS Information. [Available online from http://maps.fsl.noaa.gov.]

——, and Coauthors, 1998: The operational RUC-2. Preprints, *16th Conf. on Weather Analysis and Forecasting,* Phoenix, AZ, Amer. Meteor. Soc., 249–252.

Bloom, S. C., L. L. Takacs, A. M. DaSilvia, and D. Ledvina, 1996: Data assimilation using incremental analysis updates. *Mon. Wea. Rev.,* **124,** 1256–1271.

Boyd, B. F., W. P. Roeder, J. B. Lorens, D. S. Hazen, and J. W. Weems, 1995: Weather support to pre-launch operations at the Eastern Range and Kennedy Space Center. Preprints, *Sixth Conf. on Aviation Weather Systems,* Dallas, TX, Amer. Meteor. Soc., 135–140.

Bratseth, A., 1986: Statistical interpolation by means of successive corrections. *Tellus,* **38A,** 439–447.

Brewster, K., 1996: Application of a Bratseth analysis scheme including Doppler radar data. Preprints, *15th Conf. on Weather Analysis and Forecasting,* Norfolk, VA, Amer. Meteor. Soc., 92–95.

Brody, F. C., R. A. Lafosse, D. G. Bellue, and T. D. Oram, 1997: Operations of the National Weather Service Spaceflight Meteorology Group. *Wea. Forecasting,* **12,** 526–544.

Carpenter, R. L., K. K. Droegemeier, G. M. Bassett, S. S. Weygandt, D. E. Jahn, S. Stevenson, W. L. Qualley, and R. Strasser, 1999: Storm-scale numerical weather prediction for commercial and military aviation. Part I: Results from operational tests in 1999. Preprints, *Eighth Conf. on Aviation, Range, and Aerospace Meteorology,* Dallas, TX, Amer. Meteor. Soc., 209–211.

Case, J., 1999: Simulation of a real-time Local Data Integration System over east-central Florida. NASA Contractor Report CR-1999-208558, Kennedy Space Center, FL, 46 pp. [Available from ENSCO, Inc., 1980 N. Atlantic Ave., Suite 230, Cocoa Beach, FL 32931.]

Cole, R. E., and W. W. Wilson, 1995: ITWS gridded winds product. Preprints, *Sixth Conf. on Aviation Weather Systems,* Dallas, TX, Amer. Meteor. Soc., 384–388.

desJardins, M. L., K. F. Brill, and S. S. Schotz, 1991: Use of GEMPAK on UNIX workstations. Preprints, *Seventh Int. Conf. on Interactive Information and Processing Systems for Meteorology, Oceanography, and Hydrology,* New Orleans, LA, Amer. Meteor. Soc., 449–453.

Droegemeier, K. K., and Coauthors, 1996: The 1996 CAPS spring operational forecasting period: Realtime storm-scale NWP, Part I: Goals and methodology. Preprints, *11th Conf. on Numerical Weather Prediction,* Norfolk, VA, Amer. Meteor. Soc., 294–296.

——, and Coauthors, 1999: The explicit numerical prediction of an intense hailstorm using WSR-88D observations: The need for real time access to Level II data and plans for a prototype acquisition system. Preprints, *15th Int. Conf. on Interactive Information and Processing Systems (IIPS) for Meteorology, Ocean-*

ography, and Hydrology, Dallas, TX, Amer. Meteor. Soc., 295–299.

Ernst, J. A., and F. J. Merceret, 1995: The Applied Meteorology Unit: A tri-agency applications development facility supporting the Space Shuttle. Preprints, *Sixth Conf. on Aviation Weather Systems*, Dallas, TX, Amer. Meteor. Soc., 266–269.

Evans, J. E., and E. R. Ducot, 1994: The Integrated Terminal Weather System (ITWS). *Linc. Lab. J.*, **7,** 449–474.

Forsythe, J. M., T. H. Vonder Haar, and D. L. Reinke, 2000: Cloud-base height estimates using a combination of meteorological satellite imagery and surface reports. *J. Appl. Meteor.*, **39,** 2336–2347.

Friday, E. W., Jr. 1994: The modernization and associated restructuring of the National Weather Service: An overview. *Bull. Amer. Meteor. Soc.*, **75,** 43–52.

Gandin, L. S., 1963: *Objective Analysis of Meteorological Fields.* Gidrometeorologischøskoe Izdatelstvo. English translation by Israel Program for Scientific Translations (1965), 242 pp.

Hoke, J. E., and R. A. Anthes, 1976: The initialization of numerical models by a dynamical initialization technique. *Mon. Wea. Rev.*, **104,** 1551–1556.

Klazura, E. G., and D. A. Imy, 1993: A description of the initial set of analysis products available from the NEXRAD WSR-88D system. *Bull. Amer. Meteor. Soc.*, **74,** 1293–1311.

Lin, Y., P. S. Ray, and K. W. Johnson, 1993: Initialization of a modeled convective storm using Doppler radar-derived fields. *Mon. Wea. Rev.*, **121,** 2757–2775.

Manobianco, J., and J. Case, 1998: Final report on prototype local data integration system and central Florida data deficiency. NASA Contractor Report CR-1998-208540, Kennedy Space Center, FL, 57 pp. [Available from ENSCO, Inc., 1980 N. Atlantic Ave., Suite 230, Cocoa Beach, FL 32931.]

McGinley, J. A., 1995: Opportunities for high-resolution data analysis, prediction, and product dissemination within the local weather office. Preprints, *14th Conf. on Weather Analysis and Forecasting*, Dallas, TX, Amer. Meteor. Soc., 478–485.

McPherson, R., 1999: The future of the North American radiosonde network. Preprints, *Third Symp. on Integrated Observing Systems*, Dallas, TX, Amer. Meteor. Soc., 14–17.

NASA–JSC, 2000: Space Shuttle operational flight rules (NSTS-12820). PCN-11, Vol. A, NASA–Johnson Space Center, Houston, TX, 1532 pp. [Available from JSC/DA8, Houston, TX 77058.]

NWS, 1997: Aviation terminal forecasts. Operations Manual Chapter D-31 U.S. Department of Commerce, National Oceanic and Atmospheric Administration, National Weather Service, Silver Spring, MD, 117 pp.

——, 2000: Florida fire weather operating plan, 2000. U.S. Department of Commerce, National Oceanic and Atmospheric Administration, National Weather Service, Ruskin, FL, 60 pp. [Available from the National Weather Service, 2525 14th Avenue SE, Ruskin, FL, 33570-5468.]

Pielke, R. A., and Coauthors, 1992: A comprehensive meteorological modeling system—RAMS. *Meteor. Atmos. Phys.*, **49,** 69–91.

Priselac, E., J. E. Sardonia, and T. C. Adang, 1997: Operational weather support for NASA Space Shuttle ferry flights. Preprints, *Seventh Conf. on Aviation, Range, and Aerospace Meteorology*, Long Beach, CA, Amer. Meteor. Soc., 35–39.

Roeder, W. P., J. E. Sardonia, S. C. Jacobs, M. S. Hinson, A. A. Guiffrida, and J. T. Madura, 1999: Avoiding triggered lightning threat to space launch from the Eastern Range/Kennedy Space Center. Preprints, *Eighth Conf. on Aviation, Range, and Aerospace Meteorology*, Dallas, TX, Amer. Meteor. Soc., 120–124.

Rogers, E., T. L. Black, D. G. Deaven, and G. J. DiMego, 1996: Changes to the operational ''early'' Eta analysis/forecast system at the National Centers for Environmental Prediction. *Wea. Forecasting*, **11,** 391–413.

Shapiro, A., and J. J. Mewes, 1999: New formulations of dual-Doppler wind analysis. *J. Atmos. Oceanic Technol.*, **16,** 782–792.

Snook, J. S., P. A. Stamus, and J. Edwards, 1998: Local-domain analysis and forecast model support for the 1996 Centennial Olympic Games. *Wea. Forecasting*, **13,** 138–150.

Sun, J., and N. A. Crook, 1996: Comparison of thermodynamic retrieval by the adjoint method with the traditional retrieval. *Mon. Wea. Rev.*, **124,** 308–324.

Walko, R. L., W. R. Cotton, J. L. Harrington, and M. P. Meyers, 1995: New RAMS cloud microphysics parameterization. Part I: The single-moment scheme. *Atmos. Res.*, **38,** 29–62.

Wilson, J. W., and D. L. Megenhardt, 1997: Thunderstorm initiation, organization, and lifetime associated with Florida boundary layer convergence lines. *Mon. Wea. Rev.*, **125,** 1507–1525.

Xue, M., K. K. Droegemeier, and V. Wong, 2000: The Advanced Regional Prediction System (ARPS)—A multi-scale nonhydrostatic atmospheric simulation and prediction model. Part I: Model dynamics and verification. *Meteor. Atmos. Phys.*, **75,** 161–193.

——, and Coauthors, 2001: The Advanced Regional Prediction System (ARPS)—A multi-scale nonhydrostatic atmospheric simulation and prediction tool. Part II: Model physics and applications. *Meteor. Atmos. Phys.*, **76,** 143–165.

Zhang, J., F. H. Carr, and K. Brewster, 1998: ADAS cloud analysis. Preprints, *12th Conf. on Numerical Weather Prediction*, Phoenix, AZ, Amer. Meteor. Soc., 185–188.